Multi-Spacecraft Observations of the Auroral Acceleration Region

SOHEIL SADEGHI

Doctoral Thesis
School of Electrical Engineering
Royal Institute of Technology
Stockholm, Sweden, 2012

The cover picture shows aurora australis viewed from international space station (Courtesy ISS- NASA)

Space and Plasma Physics
TRITA-EE 2012:048 School of Electrical Engineering, KTH
ISSN 1653-5146 SE-10044 Stockholm
ISBN 978-91-7501-526-2 SWEDEN

Akademisk avhandling som med tillstånd av Kungl Tekniska högskolan framlägges till offentlig granskning för avläggande av Doctorsexamen i fysikalisk elektroteknik onsdagen den 21 Nov. 2012 klockan 13.00 i Sal. H1, Teknikringen 33, Kungl Tekniska Högskolan, Stockholm.

Tryck: Universitetsservice US- AB

Abstract

The two major agents for producing aurora are generally believed to be the quasi-static parallel electric fields, accelerating electrons in the auroral acceleration region (AAR), and Alfvén waves. The Cluster spacecraft quartet has made multi-spacecraft measurements in the AAR possible for the first time. Four event studies are included and discussed in this thesis, using Cluster data inside and at the top of the AAR, to address various open issues regarding the nature of the quasi-static electric potential structures, such as their altitude distribution, temporal and spatial variability, as well as their interactions with regions of Alfvén wave activity.

In Paper 1, Cluster data from the upper and lower parts of the AAR were used to determine the altitude and latitude distribution of the acceleration potential above the aurora and to address its stability in space and time. The acceleration potential pattern derived consisted of two equally broad and intense U-shaped electric potential structures and a narrower S-shaped potential structure located below. The acceleration potential distribution was found to be stable, both in intensity and width, over five minutes. Furthermore, the perpendicular (to the magnetic field) spatial scale of the electric field was found to be much smaller than that of the current in the lower AAR, but roughly equal in the upper AAR. Revealing of these features was possible only by combining data from the two Cluster spacecraft.

In Paper 2, the spatial and temporal characteristics and development of two AAR structures were studied, benefiting from a magnetic conjunction between two of the Cluster spacecraft and a short time difference (~1 min) between the spacecraft crossings. The configuration allowed for estimating the characteristic times of development for the two structures and the parallel electric field and potential drop for the more stable one. Potential structure 1, having a perpendicular width of ~80 km was short-lived, developing in less than 40 seconds and decaying in one minute. The parallel potential drop between 1.13 and 1.3 R_E altitudes increased, whereas that above 1.3 R_E remained almost unchanged during this time. For potential structure 2, having a width of ~50 km, the parallel potential drop increased by a factor of 3 below 1.3 R_E during ~40 seconds, after which it remained stable for at least a minute. Also here, the parallel potential drop above 1.3 R_E remained roughly unchanged. An average parallel electric field was estimated to be 0.56 mV/m.

In the auroral zone, the quasi-static properties are dominant in the plasma sheet (PS) and especially in the central plasma sheet (CPS), while the Alfvénic properties are generally strongest at the plasma sheet boundary layer (PSBL). Therefore it is of special interest to study the PSBL/CPS boundary, regarding how the two processes interact. In Papers 3 and 4 we addressed this matter. In each event, data from the Cluster fleet making an equatorward crossing of the high-altitude AAR were used together with a DMSP UV image of the oval. The particle and field data were used to infer the acceleration potentials of the observed arcs and their distribution in altitude and latitude. In Paper 3, observations demonstrate a quasi-static potential structure extending into the Alfvénic region of the polar cap boundary (PCB). The associated density cavity did not extend into the Alfvénic region, suggesting that the Alfvénic activity observed within the PCB region prevents the cavity formation. The results show that Alfvénic and quasi-static acceleration operate jointly in the PCB region. In Paper 4, Cluster passed over a system of East-West aligned auroral arcs. The upper extent of the AAR was found to be at least 0.5 R_E higher in altitude than generally expected. Overlapping Alfvénic and quasi-static regions were found within the PSBL and inside Region 2 of downward currents. Growth of small-scale potential structures was observed in the PSBL and in the middle of Region 2, during the ~1.5 minutes between the Cluster 4 and Cluster 3 passages. During this period, the Alfvénic regions retreated both at the poleward and equatorward oval boundaries, while the quasi-static potentials intensified.

Acknowledgements

I would like to thank my supervisor, Göran Marklund, for his wonderful scientific guidance, positive attitude, and encouragement throughout these years. My second supervisor, Tomas Karlsson, for his unique professional pedagogic methods and invaluable suggestions and discussions. I am grateful to Per-Arne Lindqvist for his supports, and especially for helping me in accessing and verifying the Cluster data. To my wonderful ex-officemates, Torbjörn Sundberg and Hanna Dahlgren, for the rich spectrum of friendship I enjoyed; I'm sure I'm not the only one who is missing them here at the SPP! To my officemate, Nicola Schlatter. To Nickolay Ivchenko and Anita Kullen for great discussions. The former colleagues, Sonia Lileo and Tommy Johansson, for their inspiring works, which I learned from. To Judy Cumnock for her kind advises on the DMSP data. To Lars Blomberg, Michael Raadu, Johanna Bergman, Ola Carlström, Stig Rydman, Göran Olsson, Jonas Olson, and Irene Kindblom, for supporting me in different ways; and to my friends, Quing Huo, and Bin Li.

I am thankful to my family and friends, for their never-ending support.

The work was supported by the Swedish National Space Board and the Space and Plasma Physics, School of Electrical Engineering, KTH.

List of Papers

This thesis is based on the work presented in the following papers.

1. G. T. Marklund, **S. Sadeghi**, T. Karlsson, P.-A. Lindqvist, H. Nilsson, C. Forsyth, A. Fazakerley, E. A. Lucek, and J. Pickett (2011). Altitude Distribution of the Auroral Acceleration Potential Determined from Cluster Satellite Data at Different Heights. Phys. Rev. Lett. 106, 055002, doi:10.1103/PhysRevLett.106.055002.

2. **S. Sadeghi**, G. T. Marklund, T. Karlsson, P.-A. Lindqvist, H. Nilsson, O. Marghitu, A. Fazakerley, and E. A. Lucek (2011). Spatio-temporal Features of the Auroral Acceleration Region as Observed by Cluster. J. Geophys. Res. 116, A00K19, doi:10. 1029/2011JA016505.

3. G. T. Marklund, **S. Sadeghi**, J. A. Cumnock, T. Karlsson, P-A. Lindqvist, H. Nilsson, A. Masson, A. Fazakerley, E. Lucek, J. Pickett, and Y. Zhang (2011), Evolution in space and time of the quasi‐static acceleration potential of inverted‐V aurora and its interaction with Alfvénic boundary processes, J. Geophys. Res., 116, A00K13, doi:10.1029/2011JA016537.

4. **S. Sadeghi**, G. T. Marklund, T. Karlsson, P.-A. Lindqvist, H. Nilsson, O. Marghitu, Y. Zhang A. Fazakerley, and E. A. Lucek (2012). Cluster Observations of Quasi-Static Potential Structures Overlapping With Alfvénic Regions. Submitted to J. Geophys. Res.

These papers are hereafter refereed to as Paper 1, Paper 2, Paper 3, and Paper 4.

Publications with contributions by the author not included in this thesis:

G. T. Marklund, **S. Sadeghi**, B. Li, O. Amm, J. A. Cumnock, Y. Zhang, H. Nilsson, A. Masson, T. Karlsson, P-A. Lindqvist, A. Fazakerley, E. Lucek, and J. Pickett (2012). Cluster multi-point study of the acceleration potential pattern and electrodynamics of an auroral surge and its associated horn arc. J. Geophys. Res., in print.

Contents

Chapter 1

Introduction

The aurora represents the visible manifestation of a chain of interactions between the solar wind, the magnetosphere, and the ionosphere. The energy gained from slowing down the solar wind as it encounters the Earth's magnetosphere is transformed into field-aligned guided fluxes of charged particles, producing aurora as a result of a chain of processes. The aurora can be produced in discrete forms by accelerated particles, or in diffuse forms by precipitating particles which have not been subject to a low-altitude acceleration. The major role in the auroral particle acceleration is played by electric potential structures above the aurora. This thesis presents observational studies of these structures. Chapter 2 provides a brief introduction to plasma physics and the space environment, from the solar wind to the magnetosphere and the ionosphere. Chapter 3 is devoted to the aurora, the auroral current circuit, and the auroral acceleration region. Chapter 4 presents a brief overview of Alfvén waves, their signatures, and their role in producing aurora. In chapter 5, the Cluster spacecraft and their instruments will be described. The Cluster instruments EFW (Electric Fields and Waves), FGM (Flux Gate Magnetometer), CIS (Cluster Ion Spectroscopy), and PEACE (Plasma Electron And Current Experiment) are the main measurement tools used for the studies presented in this thesis. Chapter 6 presents brief summaries of the four papers included in this thesis. Chapter 7 introduces some future work to be done.

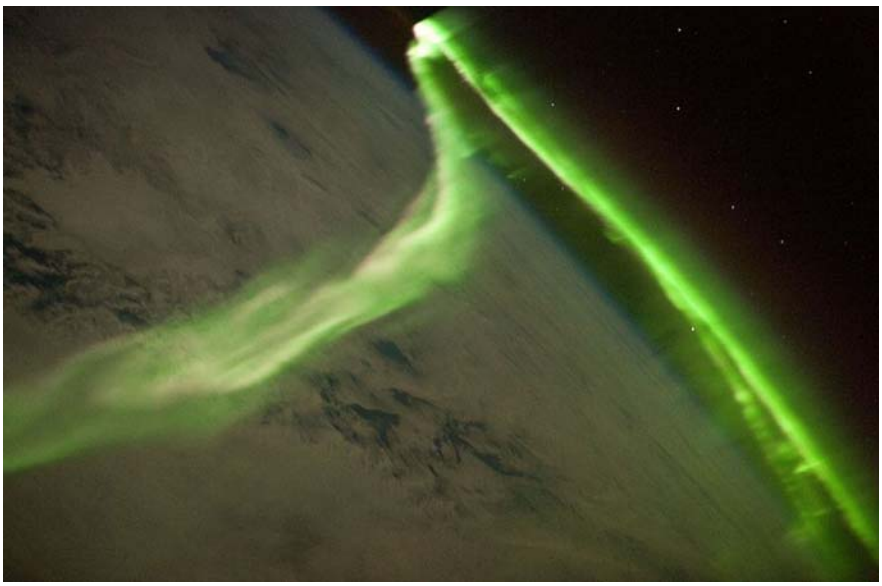

Figure 1.1: Aurora Australis on May 29, 2010, likely triggered by the interaction of the magnetosphere with a coronal mass ejection erupting from the Sun on May 24. Image taken from the ISS; adapted from NASA-Astronomy Picture Of the Day.

Chapter 2

Space plasma physics

We live in the small fraction of the universe where natural ionization of the matter is extremely unlikely, mainly due to low temperature. Outside the atmosphere however, the temperature in most of the space is so high that the matter is ionized into electrons and positive ions, exhibiting a fourth state of matter, namely the plasma state. Space physics studies include the physics of the sun, the solar wind, the interactions between the solar wind plasma and the magnetospheres of the planets, magnetosphere-ionosphere interaction, as well as auroral processes. It generally utilizes in-situ experimental data from satellites and sounding rockets, but also data from ground-based instruments like magnetometers, radars, and cameras. In this chapter, a short overview of plasma physics will be given, followed by brief descriptions of the solar wind, the Earth's magnetosphere and ionosphere, and the interactions between them.

2.1 Plasma physics

Plasma is an ionized gas of overall charge neutrality and collective behavior that is governed mainly by electromagnetic forces rather than hydrodynamic forces (Chen, 1984). A first prerequisite for an ionized gas to fit the definition of plasma is that the size of the system must be much larger than the *Debye length*:

$$L >> \lambda_D = \sqrt{\left(\varepsilon_0 k_B T_e / e^2 n\right)} \tag{2.1}$$

The Debye length λ_D is a measure of the system's ability to shield out electric potentials applied to it. The potential from a charged particle in a plasma decreases exponentially with distance so that beyond a few Debye lengths it is basically negligible. Here ε_0 is the vacuum dielectric constant, k_B is the Boltzmann constant, T_e is the temperature of the electrons, e is the electron charge, and n is the number density of the electrons. It can be shown that this also implies a close balance between ions and electrons, namely *quasi-neutrality*.

As a second condition, and for the Debye shielding to be a statistically valid concept, the *plasma parameter*, defined as the number of particles in a Debye sphere, must be much greater than one:

$$N_D = 4\pi n \lambda_D^3 / 3 >> 1 \tag{2.2}$$

The third condition for an ionized gas to behave like plasma, refers to the relative dominance of electromagnetic forces in comparison with hydrodynamic forces and requires that the collision frequency with the neutral particles is low enough:

$$\omega\tau > 1 \tag{2.3}$$

where ω is the frequency of the typical plasma oscillations and τ is the mean free time between collisions with neutral atoms.

As seen from the above brief description, a plasma is characterized by two parameters: density and temperature. In space plasmas, each of these parameters can vary over an extremely broad range.

Single-particle motion

Collisions can often be neglected in space (above ~1000 km altitude). A first approximation to understand the physics of the plasma in space is to study the motion of a single charged particle, free from interactions with other particles, in presence of external electromagnetic fields.

The force acting on a charged particle in an electromagnetic field is given by the Lorentz equation:

$$\mathbf{F} = q(\mathbf{E} + \mathbf{V} \times \mathbf{B}) \tag{2.4}$$

In a homogeneous magnetic field, **B**, and in the absence of an electric field, a particle with charge q and mass m, will gyrate around the magnetic field lines, with a *gyrofrequency* of:

$$\omega_g = \frac{qB}{m} \tag{2.5}$$

This angular frequency is also called *Larmor frequency* or *cyclotron frequency*. The radius of the gyration, the *Larmor radius*, is given by:

$$r_L = \frac{mv_\perp}{qB} \tag{2.6}$$

where $v_\perp$ is the velocity component perpendicular to **B**. This spiral motion explains how charged particles are prevented from moving freely across magnetic field lines, and for example how the Earth's magnetic field prevents the solar wind from entering its region of relative dominance.

If there is a constant magnetic field **B**, and a constant force **F**, a drift motion will be superposed on the gyro motion. The drift velocity is given by:

$$\mathbf{u}_d = \frac{\mathbf{F} \times \mathbf{B}}{qB^2} \tag{2.7}$$

The force **F** can, for example, be that from an electric field **E**, which leads to:

$$\mathbf{u}_E = \frac{\mathbf{E} \times \mathbf{B}}{B^2} \tag{2.8}$$

This drift velocity is independent of the charge, and is perpendicular to both the electric and the magnetic fields. (If there is also an electric field $E_{//}$ parallel to B, the particle will in addition to gyrating, simply be accelerated under the $F_{//} = qE_{//}$ force along the field lines.).

Any particle with charge q moving in a circular orbit with a gyrofrequency of ω_g, generates an average current $I = q\omega_g/2\pi$ in the loop and hence a *magnetic moment*: $\boldsymbol{\mu} = I\,\mathbf{A}$, where **A** is the area of the loop with the direction determined from the right hand rule. If the gyration has resulted from an external magnetic field **B** as discussed, the magnetic moment will be $\mu = q\omega_g r_L^2 / 2$, which leads to:

$$\mu = \frac{m v_\perp^2}{2B} \tag{2.9}$$

As a rough generalization of the Larmor radius formula in the case above, one can expect that if the magnetic field is not homogeneous, the Larmor radius of the motion is smaller where B is larger; an effect which leads to a drift of the gyrocenter in each cycle, and in the whole motion (See Figure 2.1 bottom row). Figure 2.1 summarizes some of particle motions perpendicular to the magnetic field.

If the magnetic field has a gradient parallel to **B**, i.e. if the magnetic field is converging or diverging, the particle will be affected depending on how transverse to the field it moves. The angle between the field lines and the particle velocity is called the *pitch angle* of the particle:

$$\alpha = arctan(v_\perp / v_{//}) \tag{2.10}$$

It can be shown that if the magnetic field variations are slow (i.e. **B** changes on time scales much larger than the gyroperiod and spatial scales much larger than the gyroradius), then the magnetic moment μ is conserved. This quantity is hence called an adiabatic invariant. Since the Earth's magnetic field is converging at the magnetic poles, as a consequence of the conservation of energy and magnetic moment, a particle approaching the Earth's magnetic dipole will be repelled by a *magnetic mirror force*, and will obtain higher and higher pitch angles so as to conserve $\sin^2\alpha / B$. Eventually, the particle is repelled back at a *mirror point* (without reaching down to the ionosphere) if it doesn't have a small enough original pitch angle; or it reaches the ionosphere, collides with the neutrals, and looses its energy by ionizing or exciting them. Particles with pitch angles smaller than the *loss cone angle* will be able to reach the ionosphere. The loss cone angle is given by:

$$\theta_{LC} = \arcsin\sqrt{B_{eq} / B_i} \tag{2.11}$$

where B_{eq} is the magnitude of the magnetic field at the equatorial footpoint of a magnetic field line, and B_i is its magnitude at the ionosphere along the same field line. A parallel electric field can accelerate electrons to high parallel velocities, decreasing their pitch angles and allowing them to reach the ionosphere and create aurora. Acceleration potential structures can provide such parallel electric fields. These structures are a main topic in this thesis and will be discussed in detail. Figure 2.2 gives a summary of some of the particle motions in the Earth's magnetic field.

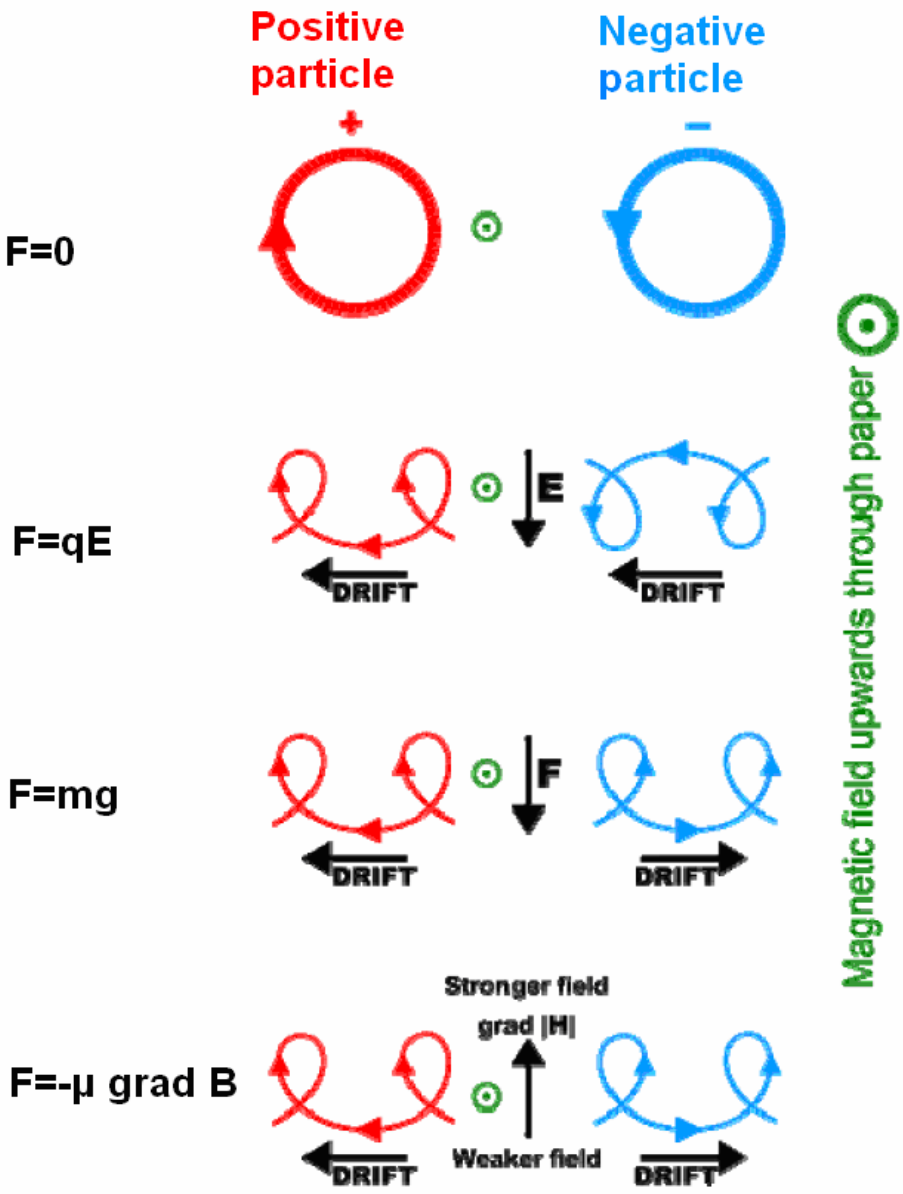

Figure 2.1: Charged particle drift motions in a magnetic field under the influence of perpendicular forces or magnetic field gradient (Figure adapted from Wikipedia; the formulae added).

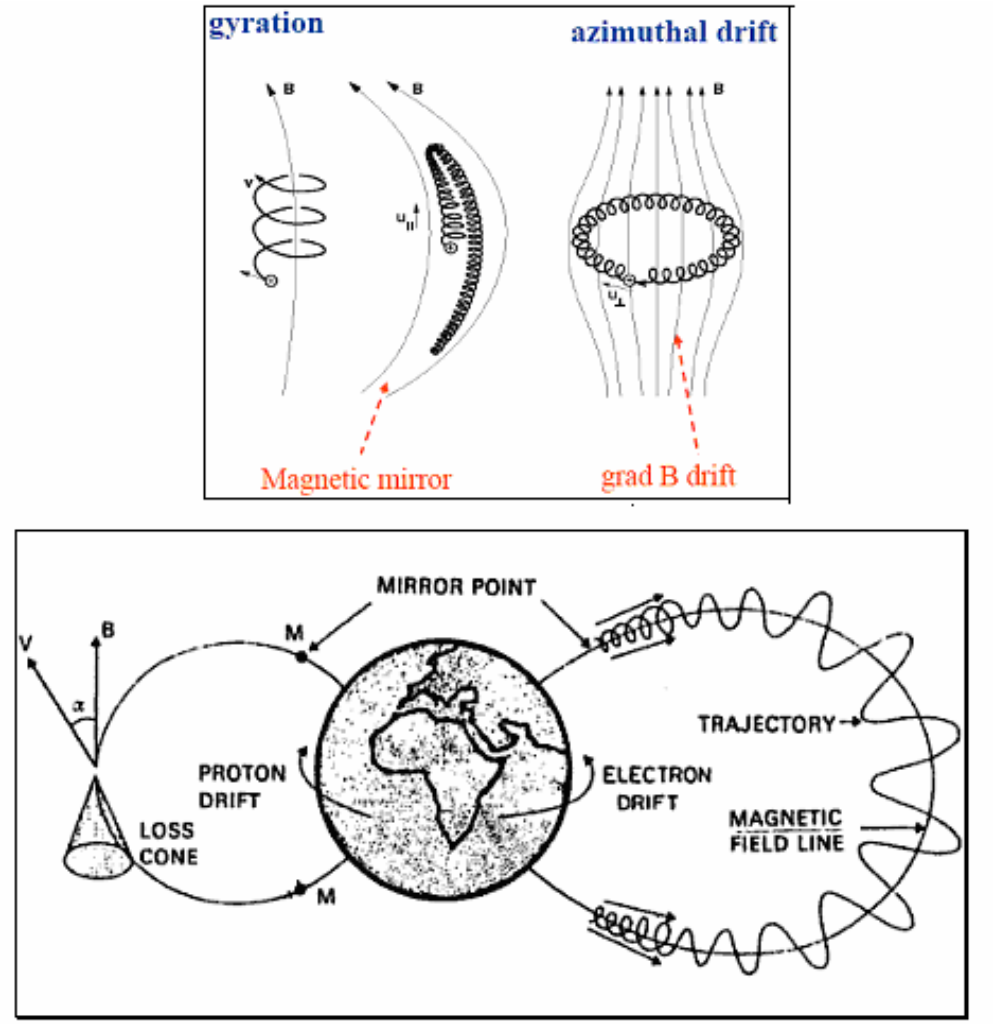

Figure 2.2: Summary of the particle motions in the Earth's magnetic field. Courtesy T. Karlsson; adapted from Lemaire (1982).

In a homogeneous thermal plasma, perturbing the system (e.g. by introducing a separation of electrons from ions) will lead to generation of an electric field which affects mainly the electrons so as to move them back to their original position, since the ions are much heavier. This leads to an oscillation of the electrons at a frequency, called the *(electron) plasma frequency*:

$$\omega_{pe} = \sqrt{e^2 n / \varepsilon_0 m_e} \tag{2.12}$$

The single-particle theory of plasmas is not applicable for calculations on current densities, temperatures or other large scale properties. In addition to this approach, there are two other basic treatments which can deal with such concepts: *kinetic theory* and *magnetohydrodynamics*.

Kinetic plasma theory

The most fundamental plasma theory, the kinetic theory, is a statistical approach which describes particles based on particle distribution functions in (six dimensional) phase-space, $f(\mathbf{r},\mathbf{v},t)$, to treat macroscopic variables. This treatment generally states that the convective derivative of the distribution function is equal to the rate of changes in it due to collisions:

$$\frac{df(\mathbf{r},\mathbf{v},t)}{dt} = \left[\frac{\partial f}{\partial t}\right]_{col} \tag{2.13}$$

The equality is called the Boltzmann equation. This rate will be zero if the collisions can be neglected. If also the forces acting on the particles are only electromagnetic, the resulting equation $df(\mathbf{r},\mathbf{v},t)/dt=0$ is called the Vlasov equation. Generally for the distribution of each species to be solved, one Vlasov equation is required (Chen, 1984).

Magnetohydrodynamics

In magnetohydrodynamics (*MHD*), the plasma is regarded as an electrically conducting fluid. By utilizing the fluid hydrodynamics equations (continuity equation, momentum equation, and state equation) in addition to the four Maxwell's equations, it comprises a set of equations to be solved for basic plasma parameters density, velocity and pressure of each species, as well as **E** and **B**. Since the ions and electrons are coupled together and the mass and momentum of the plasma is basically due to the ions, a single fluid description becomes possible. The generalized Ohm's law can be derived from such a treatment as:

$$\mathbf{E}+\mathbf{v}\times\mathbf{B} = (\mathbf{j}\times\mathbf{B}-\nabla\mathbf{P}_e)/en+\eta\mathbf{j}+(m_e/e^2n)\partial\mathbf{j}/\partial t \tag{2.14}$$

where **j** is the current density, P_e is the electron pressure tensor, and $\eta=m_e\nu_{ei}/e^2n$ is the plasma resistivity with ν_{ei} being the electron-ion collision frequency (Baumjohann and Treumann, 1999).

In the simplest case, *ideal MHD*, the fluid is assumed to have a zero resistance. If, in addition, the time variations are slow and the plasma flow is weak and highly homogeneous, the right hand side terms vanish, so that Ohm's law can be written:

$$\mathbf{E}+\mathbf{v}\times\mathbf{B}=\mathbf{0} \tag{2.15}$$

This equation is often called the condition for the *frozen-in flux* theorem, because it can be shown that the magnetic field lines appear to follow the motion of the perfectly conducting plasma. (This theorem is usually applicable to large scale phenomena in space, but not applicable to localized regions where acceleration processes occur and break down the frozen-in condition.) In such highly conductive magnetized plasma, as seen from the last equation, there is no simple relation between the electric field (which is

simply $\mathbf{E}=-\mathbf{v}\times\mathbf{B}$,) and the currents which are related to the magnetic field (by Ampere's law), pressure gradients and flow velocity. One important outcome of the frozen-in flux theorem is that the electric field will have only a perpendicular component; $E_{//}=0$.

The *plasma beta parameter,* defined as the ratio of plasma particle (thermal) pressure to the magnetic pressure, is usually used as a measure of whether the magnetic field lines will follow the plasma ($\beta>>1$) or the plasma will follow the motion of the field lines ($\beta<<1$).

$$\beta=p/(B^2/2\mu_0) \tag{2.16}$$

where μ_0 is the magnetic permeability of vacuum.

For non-zero resistance, from Ohm's law $\mathbf{j}=\sigma(\mathbf{E}+\mathbf{v}\times\mathbf{B})$, Ampere's law $\nabla\times\mathbf{B}=\mu_0\mathbf{j}$, and Faraday's law $\nabla\times\mathbf{E}=-\partial\mathbf{B}/\partial t$, it can be shown that: $\partial\mathbf{B}/\partial t=\nabla\times(\mathbf{v}\times\mathbf{B})+\nabla\cdot\nabla B/\mu_0\sigma$. The time rate of change of **B** is controlled by two terms: A convection term which involves the fluid velocity, and a diffusion term which involves conductivity. Usually one or the other term dominates. The magnetic Reynolds number is an estimate of the ratio between these two terms and is defined as below:

$$R_m=\mu_0\sigma UL \tag{2.17}$$

where σ is the conductivity, L is a characteristic length scale of the spatial gradients, and U is a characteristic velocity of the plasma. If $R_m>>1$, the convection term dominates and the frozen-in magnetic field flux follows the plasma convection. If $R_m<<1$, the diffusion term dominates and the field lines may change path from one plasma sample volume to another one. For most geophysical and astrophysical applications, $R_m>>1$ is the case. However, even in such large scale systems, this concept sometimes breaks down in small localized regions, where the scale size L (and hence R_m) becomes very small.

A plasma can also support a large number of types of waves. In 1942 Hannes Alfvén stated that "If a conducting liquid is placed in a constant magnetic field, every motion of the liquid gives rise to an EMF which produces electric currents. Owing to the magnetic field, these currents give mechanical forces which change the state of motion of the liquid. Thus a kind of combined electromagnetic-hydrodynamic wave is produced" (Alfvén, 1942). He showed that in such cases a wave will propagate along the background magnetic field, $\mathbf{B}_0$, at a speed:

$$V_A=\frac{B_0}{\sqrt{\mu_0\rho}} \tag{2.18}$$

where ρ is the mass density. This is the characteristic velocity at which the magnetic field perturbations travel along the magnetic field line; called the *Alfvén velocity*.

2.2 The near-earth space environment

The aurora is a result of the solar wind-magnetosphere-ionosphere interaction chain. In this section we discuss each of these components briefly.

2.2.1 The solar wind

The sun is made up of about 90% protons, 10% ionized Helium and traces of other elements, and neutralizing electrons; with the fusion reaction continuously converting the protons into Helium nuclei, releasing energy. The upper atmosphere of the sun, the solar corona, is at a pressure much higher than the interstellar pressure and ejects a stream of highly conductive plasma, called the *solar wind*. The speed of the solar wind is typically between 200 and 1000 km/s at the Earth's orbit, i.e. the solar wind is supersonic (the sound speed is about 50 km/s) and super-Alfvénic (the Alfvén velocity in the solar wind is about 40 km/s). At a distance of 1 AU from the sun, typical solar wind plasma properties are $n_p \approx 6.6$ cm^{-3}, $n_e \approx 7.1$ cm^{-3}; $T_p \approx 10$ eV, $T_e \approx 12$ eV. The solar wind includes also a small percentage of ionized Helium (0.25 cm^{-3}). The frozen-in magnetic field of the sun spreads out into the interplanetary space with the solar wind, as the *Interplanetary Magnetic Field (IMF)*, which is one of the most important parameters in the interaction of the solar wind with the Earth's magnetic field. The IMF vertical (Northward or Southward) component B_z, which is typically less than 10 nT at the Earth's orbit, has a key role in the interaction of the solar wind with the Earth's magnetosphere. The sun's magnetic activity, the number of sunspots, and the amount of radiation emitted by the sun change periodically with an eleven-year *solar cycle*, or *sunspot cycle*, defining the *solar minimum* and *solar maximum*.

2.2.2 The Earth's magnetosphere

The Earth's magnetic field is approximately a dipole shaped magnetic field with the dipole axis directed from the South magnetic pole (close to the North geographic pole) to the North magnetic pole (close to the South geographic pole) and tilted about 11 degrees from the Earth's rotation axis. At the surface, it has a magnitude of 62 μT at the magnetic pole, and about 31 μT at the equator. The terrestrial magnetic field works like a shield against the solar wind at distances close to the Earth. The Earth's *magnetosphere* is the region where the Earth's magnetic field has the major control of the space plasma environment around Earth. Since the solar wind properties are variable and especially the vertical component of the IMF changes direction, the shape and size of the magnetosphere are subject to continuous changes. Figure 2.3 shows an illustration of the Earth's magnetosphere during Southward IMF conditions.

The magnetosphere is compressed by the solar wind on the day side, forming the boundary of the magnetosphere, namely the *magnetopause*. It is typically located at a geocentric distance of about 10 R_E on the day side, but can be compressed towards the Earth even down to below the geostationary orbit (which is ~6.6 R_E geocentric distance). The magnetopause extends out to unknown distances of at least hundreds of Earth radii

on the night side in the tail. It is a current sheet separating the weakly magnetized, high pressure solar wind from the highly magnetized thin plasma on the Earth side (Paschmann et al., 2002). The shock wave formed at the boundary between the supersonic, super-Alfvénic solar wind and the subsonic flows of compressed plasma, is called the *bow shock*. The region of subsonic solar wind plasma is called the *magnetosheath*. The magnetosphere lies inside the magnetosheath, and can be divided into distinct regions depending on the plasma characteristics and the topology of the magnetic field.

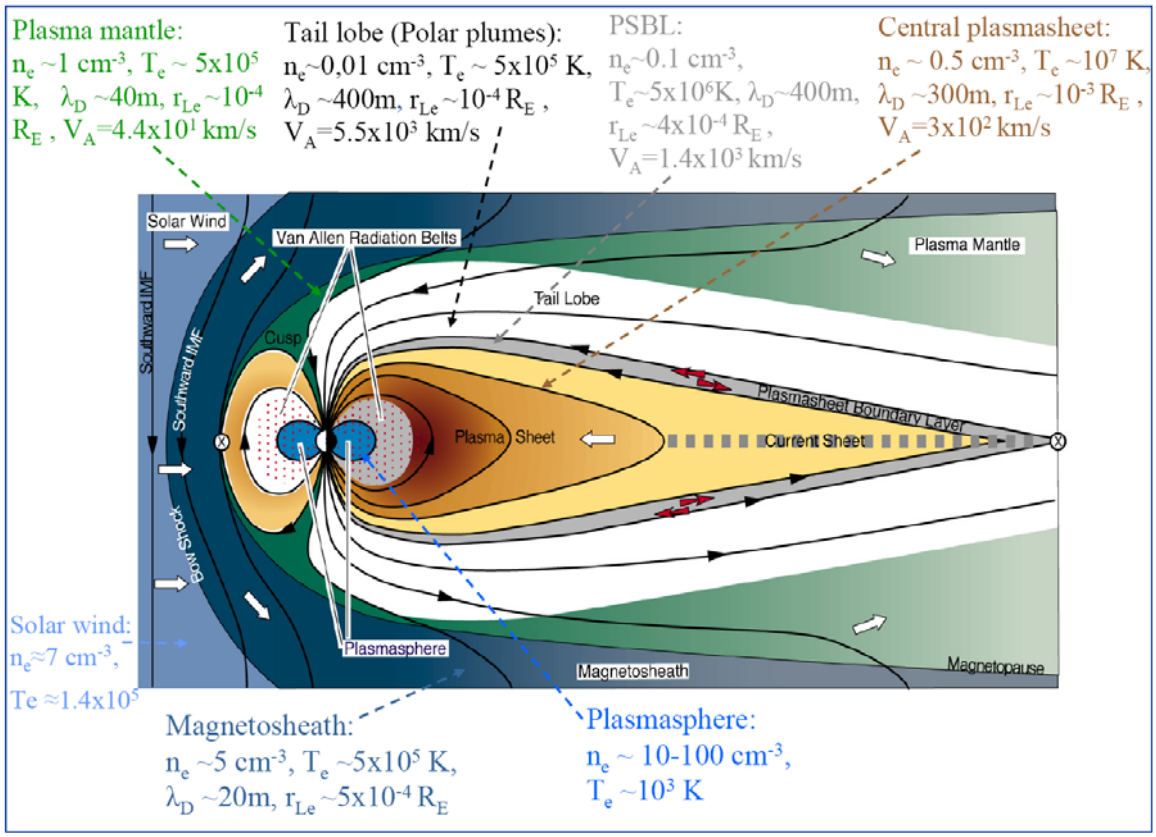

Figure 2.3: An illustration of the Earth's magnetosphere during Southward IMF conditions, with some of the plasma properties of different regions. The sun is to the left of the picture. Figure adapted from Hill and Dressler (1991). The number densities, electron temperatures, Debye lengths, electron gyroradii, and Alfvén velocities are adapted from Olsson (1997).

The region closest to the Earth is a torus-shaped population of cold dense plasma, at geomagnetic low and middle latitudes; called the *plasmasphere*. It has a temperature less than 0.1 eV (1 eV≡11600 ºK), i.e. almost the same as (or slightly higher than) the ionosphere, and a density of tens to hundreds of particles per cm^{-3}, essentially decreasing gradually from the ionospheric densities. The plasmasphere can be regarded as the upper continuation of the ionosphere and co-rotates with the Earth. The outer boundary of the plasmasphere is called the *plasmapause* (Kivelson and Russell, 1995). The orders-of-magnitude hotter population located on the higher latitude field lines, is called the *(central) plasma sheet*. *Van Allen radiation belts* are torus-shaped regions of highly

energetic (100 keV to hundreds of MeV) particles produced by cosmic rays by interactions with the atmosphere, and being trapped and bouncing between the geomagnetic mirrors.

In the magnetosphere, the frozen-in magnetic field condition generally holds. Two exceptions are the two *magnetic reconnection* sites and the *auroral acceleration region*, all located at thin boundaries between different plasmas. In the reconnection process, energy is essentially transferred between the magnetic field and the plasma. When the IMF vertical component is pointing Southward, at the magnetopause front side, some of the geomagnetic field lines can reconnect with the IMF, and instead of connecting to the Earth at both ends, connect to the IMF of the solar wind, and extend out. Through reconnection, the solar wind flow around the magnetosphere drives a global convection in the Earth's magnetosphere which partly couples to the ionosphere.

The magnetosphere is extended on the night side, forming a *magnetotail*. The second reconnection site is located in the far magnetotail, in the neutral current sheet separating regions of oppositely directed geomagnetic field lines. The two reconnection sites are marked by cross signs in Figure 2.3. The *tail lobe*s are the regions where the magnetic field lines map down to the *polar cap (PC)*, which is magnetically connected to the IMF (Kivelson and Russell, 1995), and is filled with very low-energy electron precipitation of solar wind origin (Paschmann et al., 2002). The density in the tail lobes (polar plumes) is very low, on the order of 0.01 cm^{-3}. The *plasma sheet boundary layer (PSBL)* is the region between the tail lobes and the plasma sheet, mapping at the equator side to the nightside auroral latitudes, and on the pole side to the *polar cap boundary* of the auroral oval (*PCB*). The background density and temperature in the PSBL vary in the range between those of the tail lobe and the plasma sheet, but embedded in this are ion and electron beams of several keV energy, carrying field-aligned-currents, both towards and away from Earth. The PSBL plasma is an important source of high-latitude aurora. The (Northern and Southern) *cusps* are the funnel-shaped regions separating the field lines that close on the day side from the field lines dragged into the tail. In the cusps, dense solar wind plasma enters the magnetosphere and down to the ionosphere.

2.2.3 The ionosphere

The ionosphere is the uppermost part of the atmosphere, ionized by solar radiation (mainly by EUV) and by precipitating charged particles (at high latitudes). It is the boundary between the completely ionized magnetosphere and the neutral atmosphere. The higher the altitude, the higher the ionizing radiation intensity, but the lower the neutral number density is. This can be expected to result in a maximum in the electron density profile in the ionosphere. By considering more details of the incident radiation spectrum, the radiation penetration depths, and the atmospheric species, the electron density profile can be obtained, typically like Figure 2.4, with peaks at different heights, namely *D, E, F1, F2 layers*.

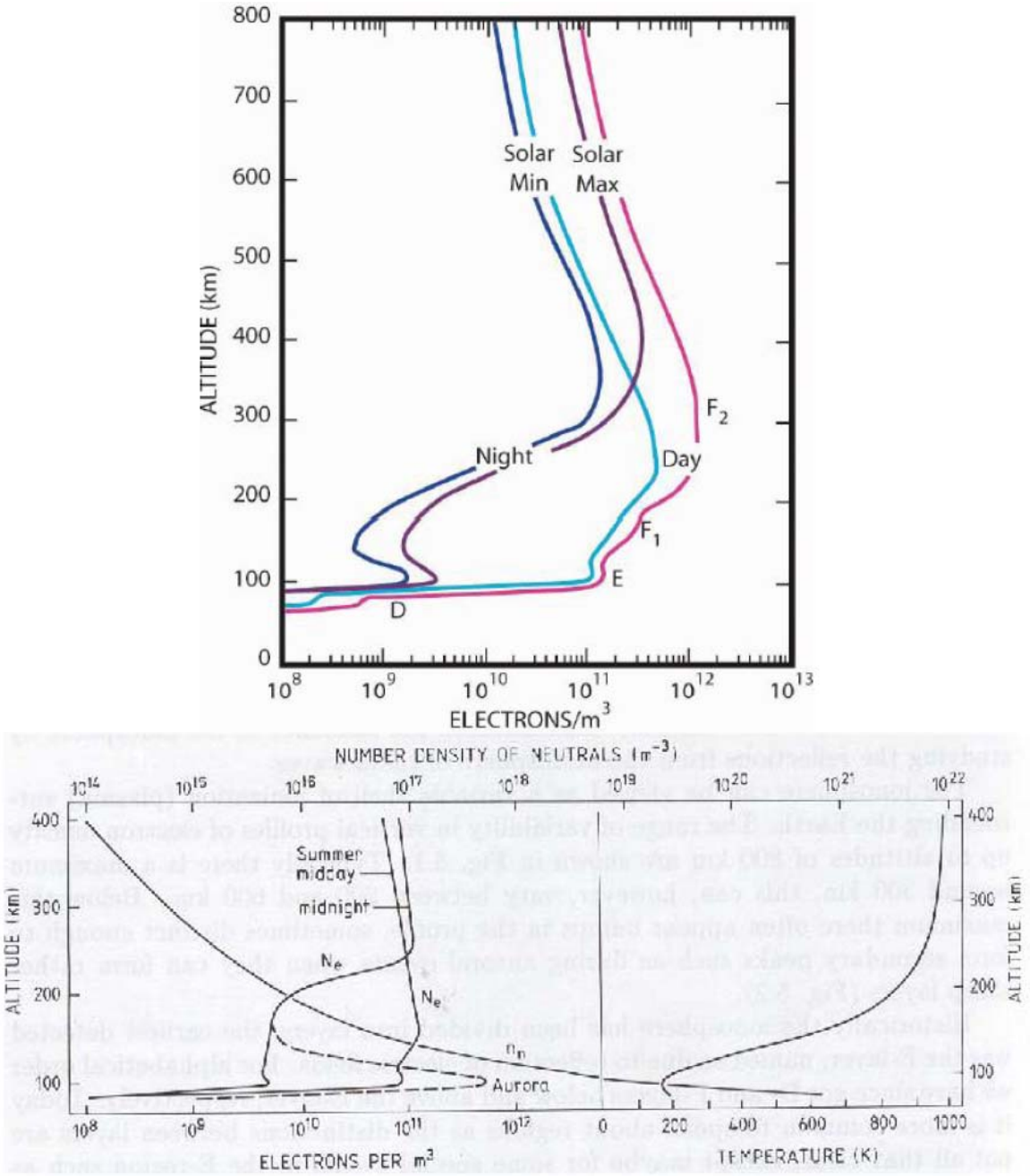

Figure 2.4: Upper panel: Typical ionospheric electron density profiles (Richmond, 1987); bottom panel: electron density profiles and a secondary auroral peak in it. Neutral density and atmosphere temperature profiles are also shown (Brekke, 1997).

The main peak in the electron density profile is located at around 300 km altitude. The secondary peak at around 100 km increases significantly during auroral activitiy, due to precipitating particles (mainly electrons) of several keV energies. As seen in the figure, ionospheric properties have diurnal changes as well as solar-activity related variations. The D, E, and F1 layers mainly disappear at night.

The plasma above the ionosphere is collisionless. The particles move freely along the field lines, and experience an **E**×**B** drift regardless of their charge and there is no net current perpendicular to the magnetic field. In the ionosphere, there are (actually dominant densities of) neutrals; the ions and electrons collide with them, even if they move along the field lines. The conductivity along the magnetic field lines (*parallel conductivity*) becomes limited by collisions with neutral particles, resulting in a rapid decrease of the parallel conductivity below 120 km. In addition, the **E**×**B** drift of the charged particles (in response to an electric field **E**) gets disrupted very often during a gyro period, and as a result, current densities can be carried transverse to the field line, although still much weaker than in the parallel direction (Paschmann et al., 2002). The conductivity in the direction along the perpendicular electric field component is called the *Pedersen conductivity,* and the conductivity in the direction perpendicular to both the magnetic and electric fields is called the *Hall conductivity*. These transverse conductivities depend highly on the ion-neutral and electron-neutral collision frequencies and vanish above 1000 km of altitude. Figure 2.5 shows typical ionospheric conductivities for night/day and solar minimum/maximum conditions.

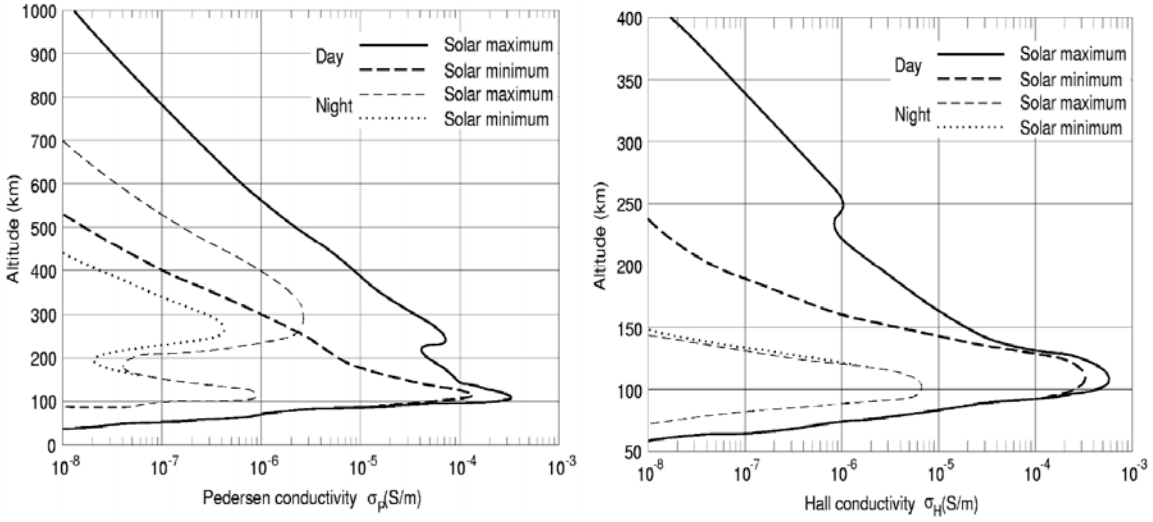

Fig. 2.5: Altitude variation of the Pedersen (left panel) and Hall (right panel) conductivities (after Hanson, 1965). Note that the vertical axis limits are not the same for the two pictures. Also note that the conductivity profiles vary considerably with local time, latitude, solar activity, and auroral activity.

The altitude region in which the ionospheric currents flow is mainly concentrated between 100 and 200 km. In fact, most of the current flow occurs within an altitude layer of less than 60 km thickness, i.e. very thin compared to the magnetospheric dimensions. Therefore it is common to use the height-integrated Pedersen and Hall conductivities (i.e. the conductances), when studying the electrodynamics of the ionosphere and its coupling with the magnetosphere.

2.3 Solar wind-magnetosphere-ionosphere interaction

The interaction between the solar wind, the magnetosphere, and the ionosphere can be roughly based on the Dungey picture of an open magnetosphere during Southward IMF times, which provides a framework demonstrating the fundamental role of reconnection, to which details may be added (Kivelson and Russell, 1995). Here we present the model briefly.

Dayside reconnection and the polar cap electric field

As noted previously, during periods of Southward IMF, reconnection processes take place. On the dayside magnetopause, the IMF field lines reconnect with the geomagnetic field lines and a large scale global plasma convection is driven by the solar wind flow in the outer magnetosphere (Figure 2.6). (The term convection was attached to this plasma flow since its two-cell pattern looks like thermally driven flows, although it is not driven by thermal effects) (Kivelson and Russell, 1995). The insert in Figure 2.6 shows the flow of the end of the field line, (from point 1 to point 6) in the Northern ionosphere. The flow of the solar wind across the interplanetary portion of the open polar cap magnetic field lines generates an interplanetary electric field $E_{SW} \sim u_{SW} B_{SW} \sim$ (400 km/s)(7 nT)~ 3 mV/m. (u_{SW} is the solar wind velocity and B_{SW} is the solar wind magnetic field). This electric field maps down along the highly conductive magnetic field lines, which can be considered as equipotentials (Lyons, 1992), leading to a dawn-dusk oriented electric field in the ionosphere across the polar cap and causes the plasma to move towards the nightside across the polar cap. From this model, the cross tail potential drop can be estimated:

$$\Delta V_{tail} \sim u_{SW} B_{SW} D_{tail} \sim 700 \text{ kV} \tag{2.19}$$

where D_{tail} is the cross-tail width, approximately about 40 R_E.

At the ionospheric side, by using ground based ionospheric measurements of plasma drift velocity u_{PC}, the cross polar cap electric field (E_{PC}) and potential drop (ΔV_{PC}), can be estimated:

$$E_{PC} = u_{PC} B_{PC} \sim (400 \text{ m/s}) (55000 \text{ nT}) \sim 22 \text{ mV/m} \tag{2.20}$$

$$\Delta V_{PC} = 2 R_{PC} E_{PC} \sim (3000 \text{ km}) (22 \text{ mV/m}) \sim 70 \text{ kV} \tag{2.21}.$$

where B_{PC} is the geomagnetic field at the polar cap (at the ionosphere) and R_{PC} is the radius of the polar cap. Such values are also confirmed by electric field observations from satellite crossings over the polar cap. It is believed that about 10% of the IMF penetrates the magnetopause, since the potential difference across the polar cap is about ten times smaller than the ~700 kV that would result from a penetration of the entire IMF across the magnetopause.

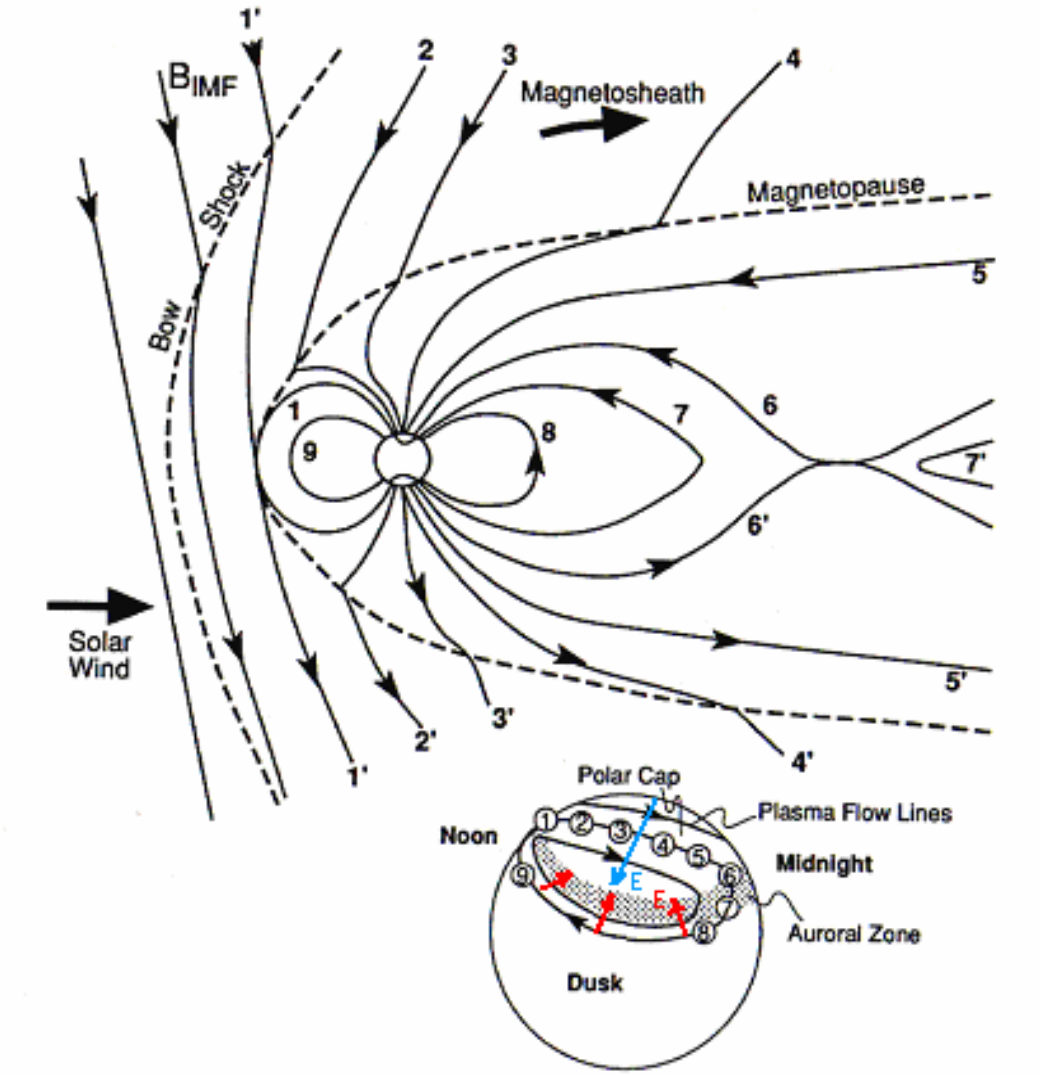

Figure 2.6: Dungey-type convection pattern of plasma within the magnetosphere, driven by reconnection. The numbered field lines show the succession of configurations of geomagnetic field line (1) after reconnecting with an IMF field line (1'), being pulled by the solar wind over the polar cap (to point 5) creating a dawn-dusk electric field in the polar cap (shown by the blue vector), reconnecting (6, 6') and moving back sunwards through the auroral oval (points 6 to 9), creating a poleward electric field on the evening sector (shown by the red vector). Adapted from Kivelson and Russell (1995).

Nightside reconnection and poleward/equatorward electric fields

The night side reconnection, between the Northern and Southern far magnetotail field lines (at ~30 R_E), brings back the reconnected field lines which are now connected at both ends to Earth at latitudes below the polar cap, i.e. in the auroral oval (from point 6 to point 9 in Figure 2.6). This convection leads to a poleward electric field in the evening sector, and an equatorward electric field in the morning sector of the auroral oval. The reconnection process will act so as to energize the plasma sheet particles.

The magnetosphere-ionosphere current system

At large scale and under undisturbed (steady state) conditions, the ionospheric electric fields and currents are coupled to the magnetosphere, a coupling mediated by upward and downward field-aligned currents (abbreviated FAC, also called Birkeland currents) as seen in Figure 2.7 (Paschmann et al., 2002).

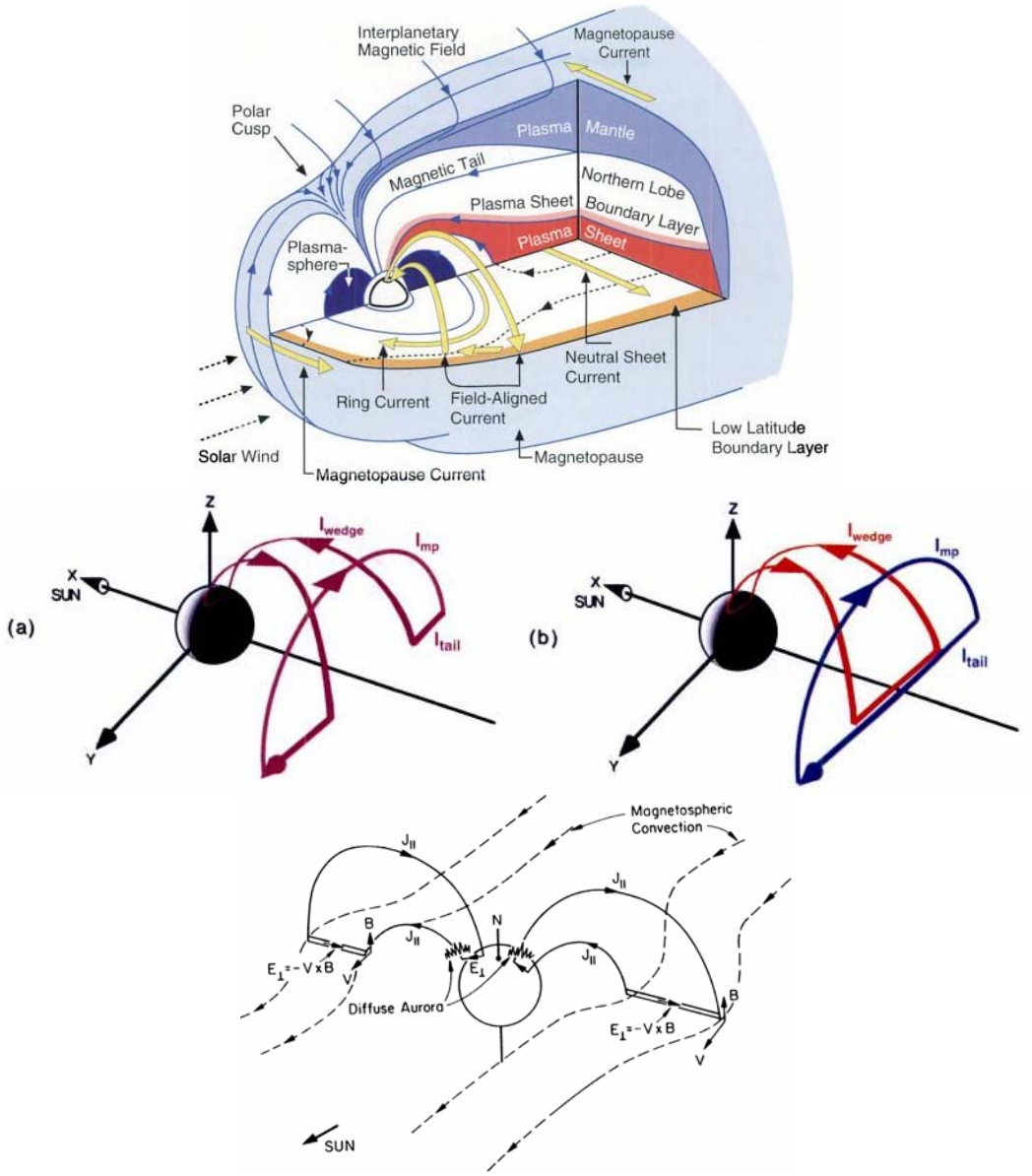

Figure 2.7: Large-scale magnetosphere-ionosphere coupling through FACs ($J_{//}$). Top panel: A 3-D view of the structure of the magnetosphere indicating the structure of the main large-scale current systems (Adapted from Kivelson and Russell, 1995); Middle panel: two possible current circuit models (only for visualization) showing the cross-tail (I_{tail}) and tail-ionosphere (I_{wedge}) currents closing by a magnetopause current I_{mp} (Figure adapted from (Paschmann et al., 2002), Bottom panel: a simplified picture showing the electric fields mapped down to the auroral oval, adapted from Kelley (1989).

The top panel of Figure 2.7 shows the main currents within the magnetosphere, the middle panel provides a 3-D picture of the substorm current wedge (SCW) system, and the bottom panel relates the currents to the generator region. These large-scale currents were first observed in satellite magnetometer data. The Pedersen and Hall ionospheric currents, which are perpendicular to the magnetic field, close the current circuit in the ionosphere by connecting the downward and upward FACs as seen in Figure 2.8. The system of FACs at the poleward side (in Figure 2.8) is called the *Region 1 currents*. The equatorward system is called the *Region 2 currents*. The Region 1 currents connect mostly to the magnetospheric boundaries while Region 2 currents close in the inner magnetosphere.

From this view, it is generally believed that the generator of the Region 1 current system is the solar wind-magnetosphere dynamo; i.e. the ionospheric current closure exerts a drag on the magnetospheric flows, establishing a magnetospheric generator ($\mathbf{E}\cdot\mathbf{j} < 0$) driving the FACs. The generator of the Region 2 currents is even less known. It is believed to be related to pressure gradients inside the magnetosphere (Paschmann et al., 2002).

The Hall currents in the ionosphere are carried by electrons and build up *Eastward and Westward Electrojets* (EEJ, WEJ) which have current densities typically between 0.5 and 1 A/m, and carry a total current of about 1 MA which may induce a detectable magnetic disturbance at the ground level. The Pedersen currents are mainly carried by ions and have a typical ionospheric current density of 0.3 to 0.5 A/m.

The direction of the electric field and the convection reverses with the reversal of the IMF direction, so that for the strongly Northward IMF, the electric field will be towards dawn on the polar cap and the plasma flow will be sunward (Lyons, 1992).

Geomagnetic disturbances

Geomagnetic disturbances and variations can be observed at geomagnetic observatories distributed around the world. *Geomagnetic storms*, are disturbances in the geomagnetic field with extended periods of large Southward IMF and high energy input into the magnetosphere. Storms link to the ring current and mainly affect the mid and equatorial latitudes, while *substorms* influence high latitude regions.

Substorms

The most frequent type of geomagnetic activity is called a (magnetospheric) *substorm*. When the IMF turns southward, a sequence of events occurs in the magnetosphere and ionosphere, driven by the increased energy input from the solar wind into the magnetosphere (Kivelson and Russell, 1995). Substorms lead to sudden changes and enhancements in the auroras and enlargement of the auroral oval. They typically last some hours and take place a few times per day. They can cause disturbances on the order

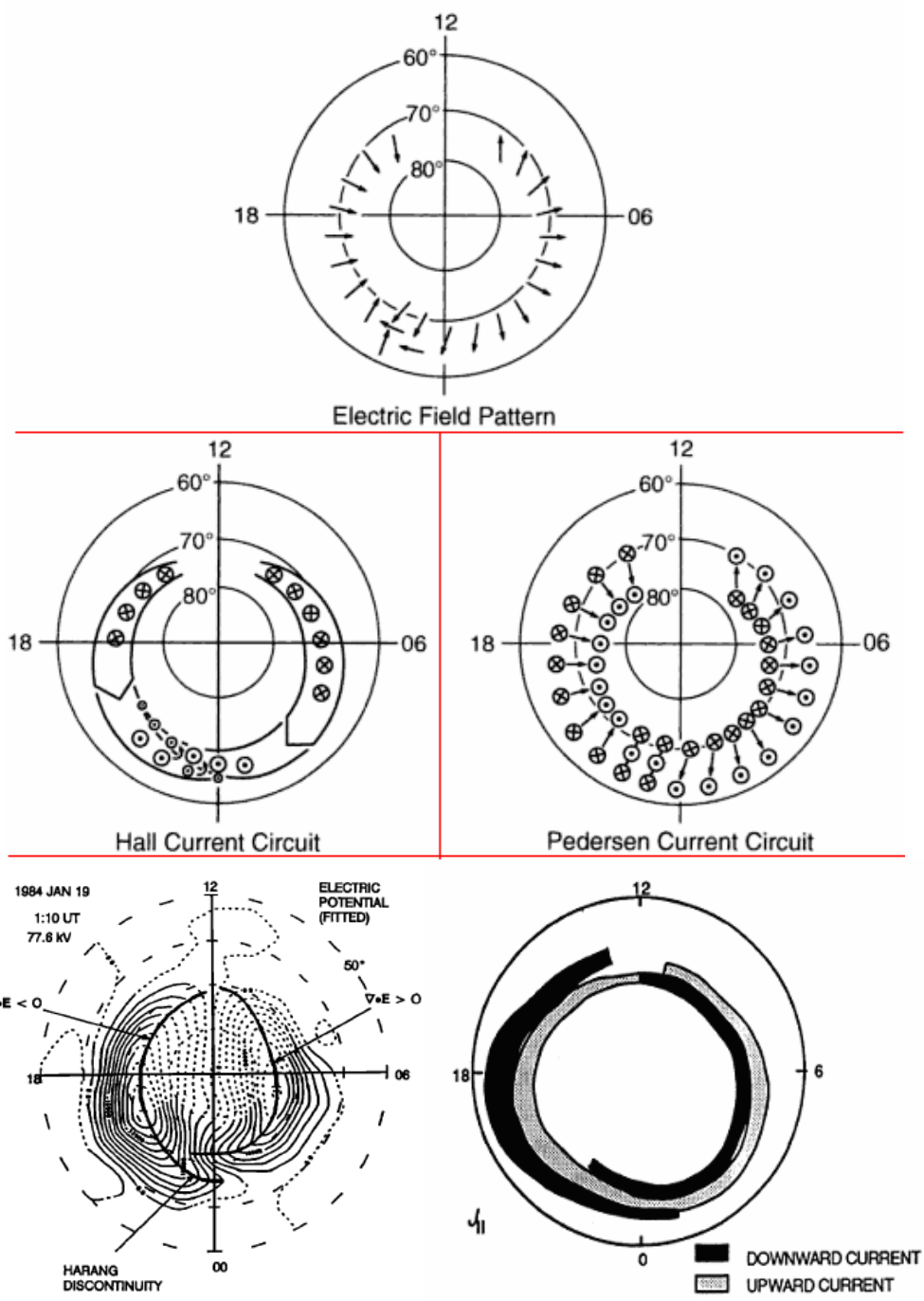

Figure 2.8: Models of ionospheric auroral oval electric field (top panel), Hall current (middle-left), and Pedersen current (middle-right) adapted from Baumjohann and Treumann (1999); along with experimental results: pattern of (converging and diverging) electric potential pattern over an entire polar cap obtained by Richmond (1988), from ground-based electric fields measurements, with dashed equipotentials where the estimated electric field uncertainties exceed 50% (lower left, Figure adapted from (Lyons, 1992); and upward and downward FAC regions (lower right), adapted from Ijima and Potemra (1978).

of a few percent of the geomagnetic field measured at Earth's surface. What triggers auroral substorms has for a long time been a key issue and matter of debate (Kivelson and Russell, 1995). Substorms are generally described by three phases which will be presented briefly based on the picture given by Baumjohann and Treumann (1999).

Growth phase: With the IMF turning southward, energy is pumped into the magnetotail by enhancement of the dayside reconnection rate, and stored as magnetic energy in the still-not-reconnected field lines in a magnetospheric long tail. This phase typically takes about one hour (Figure 2.9. top panel).

Expansion/main phase: Due to the stretched plasma sheet magnetic field lines and fast reconnection, a secondary X-line is created between the far magnetotail X-line (i.e. *distant neutral line, DNL*) and the Earth, leading to reconnection there, energizing and injecting plasma into the inner magnetosphere (and creation of a *plasmoid* on the tail side). During this phase, the geomagnetic field changes from being stretched to become more dipolar. This phase (shown in Figure 2.9 middle panel), which causes major auroral disturbances, typically lasts between half an hour and one hour. The secondary X-line is called the *near-Earth neutral line (NENL).*

Recovery phase: When the reconnection at the NENL decreases, the plasmoid and the NENL are pushed tailward and the magnetosphere gradually returns to its ground state. (Figure 2.9 bottom panel)

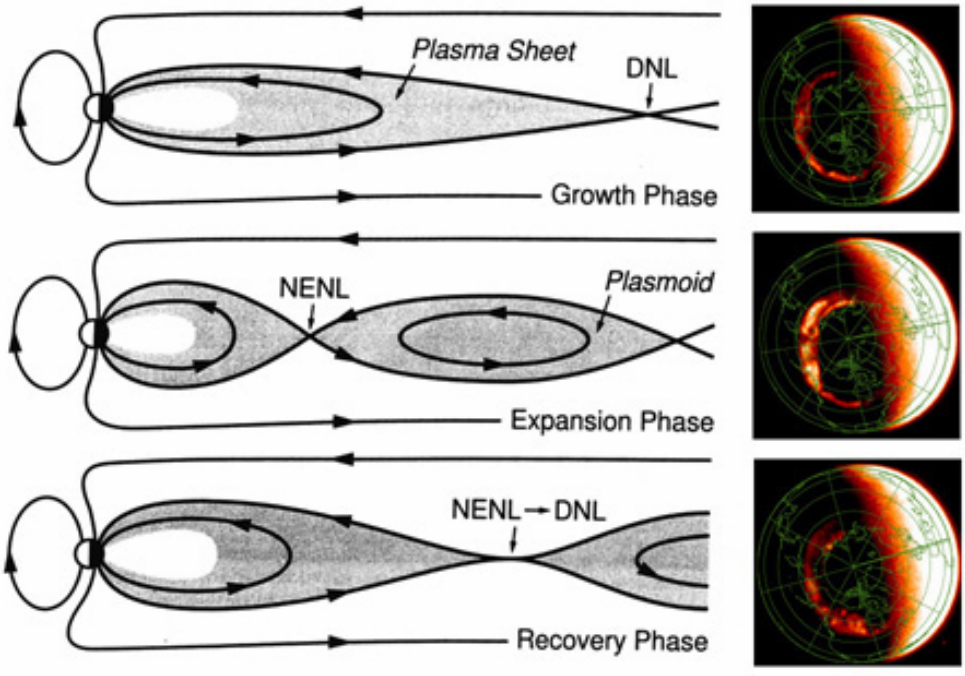

Figure 2.9: Substorm phases (The drawings are adapted from Baumjohann and Treumann (1999). The three auroral images, were obtained with the IMAGE far-UV instrument, from Southwest university Research Institute (SWRI).

The strength of a substorm is quantified by the auroral electrojet indices. The maximum poleward/equatorward magnetic field disturbance measured (on 12 different ground-based stations distributed in the Northern auroral zone) as proxy of the maximum EEJ/ WEJ current, defines the *AU/AL* index (in units of nT). The auroral electrojet (*AE*) index is defined as *AE=AU-AL*. It is widely used for research in geomagnetism, aeronomy, and solar-terrestrial physics. When the growth phase of a substorm starts, the *AE* index starts increasing. When the main (expansion) phase starts, the AE increase obtains a higher slope, and when the recovery phase starts, the AE index starts decreasing to the background (quiet-time) conditions (Figure 2.9).

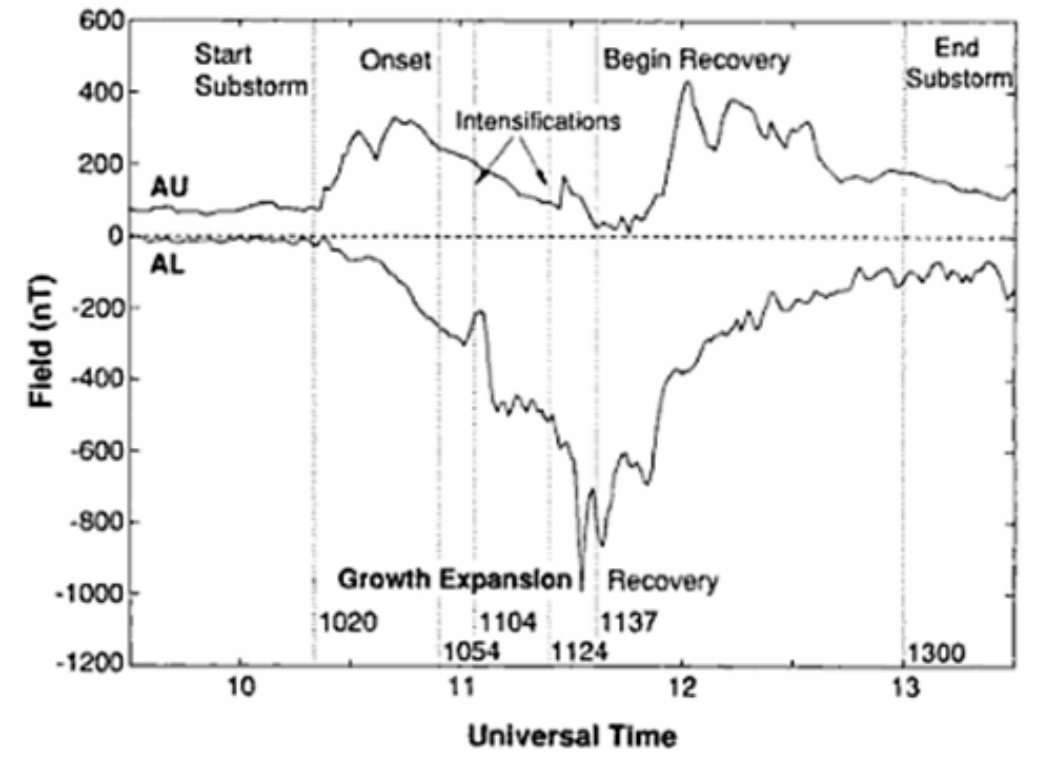

Figure 2.9: *AU* and *AL* indices for a particularly well-studied substorm. From (Kivelson and Russell, 1995).

Chapter 3

The Aurora and the Auroral Acceleration Region

The nightside auroral oval is the projection (along the magnetic field lines) of the plasma sheet on the atmosphere; however, the source particles in the plasma sheet typically require additional energy, directed along the geomagnetic field lines to overcome the magnetic mirror and reach down to the atmosphere to create visible discrete aurora. Although the aurora is known as one of the end products of the solar wind-magnetosphere-ionosphere interaction, the processes behind accelerating the electrons to such energies are still not clearly understood. This chapter introduces some of the characteristic properties of the aurora, describes some of the main theories proposed for auroral acceleration processes, and introduces the auroral acceleration region, which is a key region for understanding the auroral phenomenon, and the main focus of the four studies presented in this thesis.

3.1 Basic concepts

Auroral emissions result from the excitation of atmospheric atoms and molecules by the impinging charged particles. Almost all auroral light consists of emission lines and bands of neutral or ionized O, O_2, N, and N_2 (Paschmann et al., 2002). They are mainly caused by beams of energetic, precipitating electrons, the penetration depth of which depends on their energy. Auroral electrons typically have energies between 1 and 10 keV. The dominant emission is the green atomic oxygen line (5577 Å), at altitudes of 150 to 100 km. Electrons with lower energies cause red emissions (6300 Å, 6364 Å) around 200 km altitude. High fluxes of electrons of energies above 10 keV also give rise to red emissions, but at altitudes as low as 80 km. Two blue N_2^+ lines are 4278 Å and 3914 Å.

Visual aurora can have different forms, such as arcs, folds, spirals, curls, etc. Their sizes vary between hundreds of meters to hundreds of kilometers, and up to the size of the entire auroral oval. (Width is generally defined as the latitudinal size and length as the longitudinal size.)

In the analysis of ground-based data, an auroral *arc* generally denotes a localized brightening in visible light, normally with east-west elongation and relatively much narrower width. In the analysis of in-situ data, ‘arc’ typically refers to regions of electron precipitation with signatures of acceleration by parallel electric fields. In contrast to such arcs, *diffuse aurora* is produced by particles that are not accelerated, but only precipitate (Paschmann et al., 2002). Diffuse aurora can also be caused by protons. In this thesis, the main tools are the in-situ data and correspondingly, the category of main interest is the

large-scale auroral arc, with electron signatures, which will be discussed in more detail in the next sections.

Discrete arcs can be slightly distorted and deformed into *spirals, folds, and curls*. The main theory explaining the curl formation is the Kelvin-Helmholtz instability (Hallinan and Davis,1970; Davis and Hallinan, 1976; Hallinan,1976).

The lack of auroral emissions in a region within diffuse aurora, or intermediate between diffuse and discrete aurora is often named *black aurora* (Kimball and Hallinan, 1998).

Fine scale aurora generally have scale sizes of the order of hundreds of meters. In the studies on fine-scale aurora, different theories predict different arc thicknesses. Borovsky (1993) examined 22 theoretical mechanisms for fine-scale auroral arcs and obtained a characteristic width from each. The theoretical models all predicted auroral arc thicknesses at least an order of magnitude wider than the optically observed filaments.

3.2 Auroral arcs and the upward current region

Discrete auroral arcs are generally observed approximately tangential to the constant magnetic latitude circles, with widths of tens to hundreds of kilometers and lengths of thousands of kilometers. They are associated with upward field-aligned current sheets, typically located in the poleward part of the evening sector of the oval or equatorward part of the auroral oval morning sector, spatially associated with the locations of upward FACs in Region 1 and Region 2 (Paschmann et al., 2002). Since there are basically no collisions above the conducting ionospheric layer, the auroral magnetic field lines were theoretically viewed for years as infinitely conducting. However, due to the magnetic mirror force repelling the downgoing magnetospheric electrons and the decreasing number of current carriers at lower altitudes, there is an upper limit for the field-aligned current that can be carried by the plasma without acceleration. To maintain the current continuity (and charge neutrality), upward parallel electric fields are required; which will accelerate the electrons downward along the field lines, (decrease their pitch angle,) and enable them to reach lower altitudes. These electrons, which have gained a few keV (up to 10 keV) of energy, create the arcs. The potential drop corresponding to the parallel electric field will have its equipotential contours along the near-Earth magnetic field lines (Figure 3.1). This results in *U-shaped electrostatic potential structures*, at the bottom of which resides the parallel potential drop accelerating the electrons downward. On the two sides of such a potential structure, the electric field is converging; therefore these structures are also called *quasi-static converging potential structures* (Gurnett, 1972). The term quasi-static refers to the characteristic time of the temporal variations in the electric field which must be longer than the electron transit time across the acceleration region (i.e. the structure is stable on such a time scale). Because of the negative divergence of the electric field, these are also called *negative* potential structures. The electrons passing at the center of the structure gain more energy than those at the edges. This results in the *inverted-V* signature, which is one of the characteristics of the so-called *inverted-V arcs*. The inverted-V electrons have a relatively narrow energy distribution (called *monoenergetic electrons*), indicating that the acceleration is caused by a parallel

electric field. The peak energy of the electrons provides a measure of the potential drop on the magnetic field line above the observation point. Conversely, upgoing *beams* of accelerated ions are also usually observed with the arcs and provide a measure of the potential drop on the field line below the observation point. The downgoing electrons (i.e. above the satellite) provide information on their magnetospheric source and the upgoing ions (i.e. below the satellite) yield information about their ionospheric source (Paschmann et al., 2002).

In the altitude range where the acceleration of ions (upward) and electrons (downward) takes place, a *density cavity* is formed along the field lines.

The bipolar electric fields around such ideal inverted-V arcs are typically directed poleward and equatorward, perpendicular to the corresponding (typically east-west aligned) current sheet (Marklund, 1984).

Current-voltage relation

The maximum current density that can be carried along the auroral magnetic field lines without any resistivity or acceleration can be estimated (Lyons, 1992). Such estimates show that the upward currents can not be supplied by the ionospheric particles and hence magnetospheric electrons need to be considered. As noted before, only a small fraction of the magnetospheric electrons are in the loss cone and can contribute to the upward FAC. The field-aligned potential difference ($\Delta\Phi_{//}$) will increase this fraction. Hence, the magnitude of the FAC ($j_{//}$) should increase with $\Delta\Phi_{//}$. Assuming a Maxwellian energy distribution and an isotropic pitch angle distribution for the magnetospheric electrons, the relation between the two can be obtained (Knight, 1973) and is known as the *Knight relation*. The current also depends on the electron density, temperature, and the *mirror ratio* B_{iono}/B_{top}, which is the ratio between the ionospheric magnetic field and the magnetic field at the top of the potential difference. The relation also shows that for typical values of magnetospheric parameters, the upward FAC can not exceed 0.5 $\mu A/m^2$ with $\Delta\Phi_{//}=0$. The observed upward FACs associated with auroral arcs are typically 1 to 20 $\mu A/m^2$ and hence they demand acceleration potentials on the order of 1 to 10 kV; which is also the typical range of electron energies observed (Lyons, 1992). The Knight relation is almost linear when $1 << e\,\Delta\Phi_{//}/T_e << B_{iono}/B_{top}$, and can be written:

$$j_{//}=K\,\Delta\Phi_{//} \tag{3.1}$$

where $K=e^2 n/(2\pi m_e K_B T_e)^{1/2}$ is the Knight conductance, with n and T_e measured at the top of the potential difference in the magnetosphere.

The Knight relation, however, does not yield information about the altitude profile of the parallel potential (i.e. its distribution in altitude along the magnetic field lines). The profile depends on the plasma population features on the magnetic flux tube (Paschmann et al., 2002).

Lyons (1992) estimated a potential drop of 2.5 kV (and a natural width of ~100 km) for symmetric auroral acceleration regions, assuming a constant height-integrated Pedersen conductivity and a uniform electric field on each side of the center of the structure.

Upward parallel electric fields within negative quasi-static electric potential structures, associated with upward field-aligned currents, are mainly concentrated at altitudes between 3000 and 10000 km (Marklund, 1993; Weimer and Gurnett, 1993; Hultqvist, 1999; Lyons, 1992; and Papers 1, 2). Utilizing Viking satellite data, Marklund (1993) made a statistical estimate of the parallel electric field, which was found to be directed upward above 9000 km and downward below 3000 km altitude with average values of about 1mV/m. The region will be discussed more in section 3.6 under the name of the acceleration region.

3.3 Downward current region

Downward currents are also mainly carried by electrons. There is also evidence that to maintain the downward current continuity in a flux tube with a low number density of charge carriers, downward electric fields build up and accelerate the electrons upward, creating quasi-static *diverging (positive) potential structures* (Paschmann et al., 2002). Using Freja spacecraft data Marklund et al.1994, 1997 showed that parallel electric fields also exist in the downward current region. This was later confirmed by the FAST (Fast Auroral Snapshot Explorer) satellite data (Carlson et al., 1998). Using FAST data, Ergun (2001a) reported on the first direct observations of parallel electric fields in this region.

The current-voltage relation in the downward current region is not as clearly understood, compared to the upward current region. In contrast to the upward current region with a need to electrostatically increase the fraction of electrons in the loss cone, here the need for parallel electric field is argued to originate from the low ionospheric plasma density (Paschmann et al., 2002). Especially after the downward FAC is created and the ionosphere at the bottom of the flux tube is depleted of electrons, the ionospheric reservoir of electrons becomes empty and the Pedersen conductivity drops. To maintain the current continuity, the parallel potential drop is enhanced and the FAC sheet will widen to access the neighboring reserves farther and farther from the core of the FAC (Marklund et al., 2001; Streltsov and Marklund, 2006). Such a scenario had been numerically predicted by Karlsson and Marklund (1998).

Black aurora seen between or along discrete auroral arcs are thought to be related to downward currents and positive potential structures (Marklund et al. 1994, 1997) with parallel potentials of up to 3 kV, accelerating the electrons upward.

Downward parallel electric fields within positive quasi-static electric potential structures, sometimes associated with downward field-aligned currents, are concentrated at altitudes between 1000 and 4000 km (Marklund et al., 1997; Hultqvist, 2002).

3.4 Auroral current circuit

As stated previously, both upward and downward currents are carried mainly by electrons. The auroral current circuit consists of the upward (*primary*) current region, the downward (*return*) current region, the horizontal (perpendicular) ionospheric current connecting them, and the generator region where $\mathbf{E}\cdot\mathbf{j} < 0$. Figure 3.1 left panel shows a schematic illustration of the three lower branches of the auroral current circuit with negative and positive U-shaped electric potential structures sketched at left and right, corresponding to upward and downward field-aligned currents respectively (From Marklund et al. (2001)). The right panel shows a picture of two auroral arcs with a series of black aurora filaments in between (From Paschmann et al. (2002), courtesy T. Löfgren).

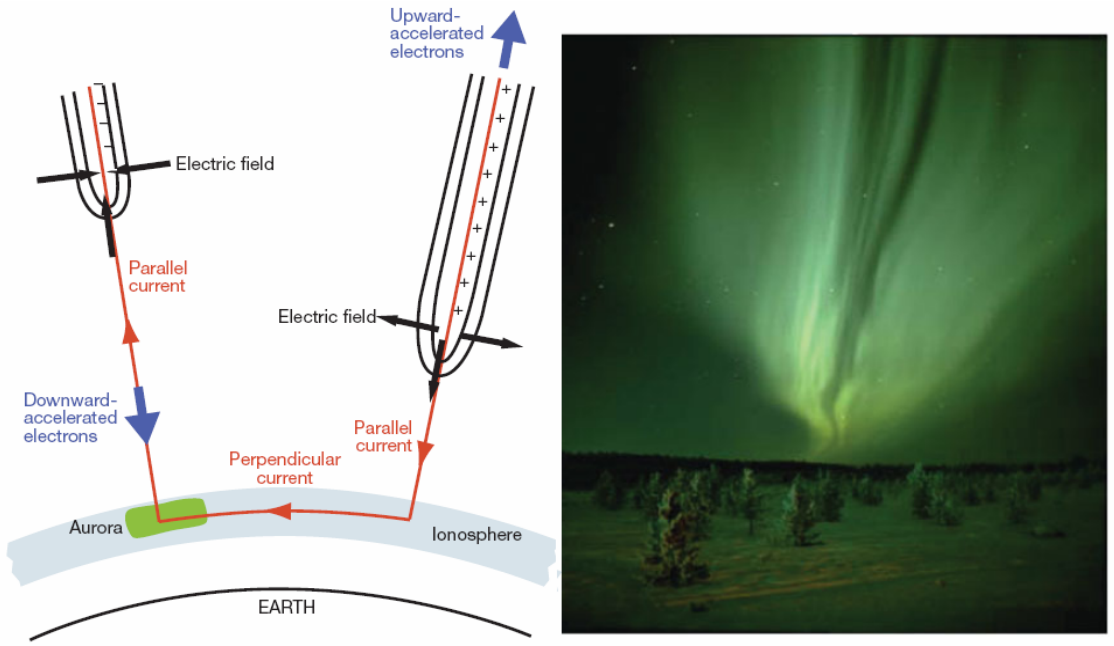

Figure 3.1: Left panel- A schematic illustration of the three lower branches of the auroral current circuit with negative and positive U-shaped electric potential structures sketched at left and right, corresponding to upward and downward field-aligned currents respectively (Adapted from Marklund et al. (2001)); Right panel- An image of two auroral arcs with black aurora filaments in between (From Paschmann et al. (2002), courtesy T. Löfgren).

3.5 Auroral particle acceleration theories

In the previous sections some of the physical processes behind the auroral particle acceleration were discussed. Here, we discuss briefly some additional properties of the quasi-static electric fields and theories behind them, followed by a concise review of the Alfvén waves and their role in particle acceleration. The main focus of this thesis is on the characteristics and dynamics of quasi-static potential structures.

3.5.1 Quasi-static electric fields

The most characteristic and dominant acceleration process for producing stable auroral forms is acceleration by quasi-static parallel potential differences (Hultqvist, 2008). In addition to the (converging or diverging) bipolar electric field signatures of the quasi-static U-shaped potential structures, *monopolar* electric fields are also observed. U-shaped potential structures are associated with situations where the magnetospheric electric field is completely decoupled from the ionospheric electric field. For *S-shaped potential structures*, the magnetospheric and ionospheric electric fields are decoupled on one side of the structure and coupled on the other side.

Practically, in negative (positive) U-shaped potential structures, the parallel potential drop inferred from upgoing ions (electrons) roughly matches the potential calculated from integrating the electric field. In S-shaped structures, there are mismatches between the two values obtained from the particle data and the electric field data, which partly has to do with the fact that the decoupling is partial.

U-shaped potential structures are typically encountered within the plasma sheet or at the equator side boundary of PSBL, at relatively soft boundaries. S-shaped potential structures are mainly associated with sharp plasma density gradients, such as at the PCB (i.e. at the poleward boundary of PSBL). This was predicted by Marklund et al. (2004) and later confirmed by Johansson et al. (2006) based on a relatively large set of Cluster data from the auroral region.

Combinations of U and S shaped structures are also possible, as observed in Paper 1. There have also been suggestions for O-shaped potential structures, with one lower-altitude and one higher-altitude parallel electric field region (Janhunen and Olsson, 2000).

The finite field-aligned potential differences (~1-10 kV), even though they are small compared to the total potential drops involved in the magnetospheric convection (~700 kV), they are enough to complicate the mapping between the electric fields in the magnetosphere and ionosphere (Kivelson and Russell, 1995). The perpendicular voltages imposed by the magnetosphere may not map down to the ionosphere perfectly and the **E×B** flows in it will slip relative to the ionospheric flows (Paschmann et al., 2002). It has been shown that large- scale electric fields with normal ionospheric widths $W_{\perp iono} >> (\Sigma_P/K)^{1/2}$ map well to the ionosphere, and that the small scale electric fields with $W_{\perp iono} << (\Sigma_P/K)^{1/2}$ do not. The ionospheric electrostatic scale length $L=(\Sigma_P/K)^{1/2}$ is termed the magnetosphere-ionosphere coupling scale length. Typical values of Σ_P =10 S and K=1 nS/m^2 yield a scale length of 100 km (Weimer, 1985; Paschmann et al., 2002); hence, generally, auroral arcs should have widths smaller than 100 km (Chaston, 2009).

Quasi-static potential structures are believed to be responsible for producing more than half of the discrete aurorae (Keiling et al., 2003; Keiling, 2009). However, it has been a question for a long time how they are distributed in altitude (In Papers 1, 2, and 4 we have results on this matter.). Numerical results suggest that the altitude of maximum

acceleration is located where the *B/n* ratio maximizes (Paschmann et al., 2002; Chaston, 2009; Lysak ,1990).

Static parallel electric field structures may be supported by a number of physical mechanisms. A concise classification of the different theories in support of a non vanishing parallel electric field can be found in Fälthammar (2004) or Karlsson (2012), a brief summary of which is presented here.

Alfvén and Fälthammar (1963) showed that a parallel electric field can be caused by the magnetic mirror provided by the dipolar shape of the Earth's magnetic field. Ergun et al., (2000) confirmed the Knight relation by using Vlasov equation simulations and FAST satellite data, and also predicted the parallel potential drop to consist of a narrow electron transition layer above which $n_e^{ionosphere}$ goes to zero, a narrow ion transition layer below which $n_i^{magnetosphere}$ goes to zero, and the intermediate altitudes in between. Mozer and Hull (2001) presented results which gave some support of this picture, using Polar spacecraft data. This explanation supports the double layer models noted below.

Double layers (DLs) consisting of charge separations with thicknesses on the order of $10\lambda_D(eV/K_BT_e)^{1/2}$, with overall quasi-neutrality, associated with a potential jump (V) between the layers, have been suggested for supporting the parallel electric field. The thickness of a DL can be on the order of kilometers for auroral plasmas, e.g. for a potential drop of a few kV and typical plasmasheet conditions.

Weak DLs, i.e. DLs associated with potential drops $V \leq K_BT_e/e$, each correspond to a potential drop of up to 1 V. It has been speculated that large numbers of them support a potential drop of several kV. They move upward along the magnetic field and might have a role in supporting the upward parallel electric field, since they are observed in association with upward- flowing ions.

Strong DLs, i.e. DLs with potential drops $V >> K_BT_e/e$, are very localized, and therefore detecting them directly is difficult. Ergun et al. (2001b) presented observations in support of strong double layers responsible for the parallel electric fields in both upward and downward current regions.

Collisionless thermoelectric effect, at the interface between hot magnetospheric plasma of plasmasheet and the cool ionospheric plasma can also create large parallel electric fields (Fälthammar, 2004; Hultqvist, 1971). The main reason is thought to be that due to the high electron velocity and inertia in the hot plasma, the flux of the electrons from the hot plasma into the cold plasma is higher than that in the opposite direction. (This imbalance in charge flux automatically builds up a potential barrier which balances the fluxes.)

Wave-particle interactions represent another means of supporting a parallel electric field. *Anomalous resistivity* is a mechanism in which the electric field of the wave impedes the motion of the electrons. The resulting parallel electric fields would be distributed over a wide altitude range. Morioka et al. (2005) estimated that for typical conditions on auroral field lines, such a process would be triggered between ~8000 and ~17,000 km of altitude.

This theory, applied to the auroral processes turned out to imply an extremely fast heating of the local plasma (Block, 1984; Cornwall and Chiu, 1982). Such a heating has not been observed, and the implied energy dissipation shortens the lifetime of the potential structure; hence this theory does not today attract much attention.

3.5.2 Alfvén wave aurora

The quasi-static picture was based on steady-state conditions of coupling between the ionosphere and the magnetosphere, i.e. the static coupling. It mainly describes steady auroral arcs. However, auroral phenomena are also known to be very dynamic exhibiting fast motions and brightness changes. Specific kinds of Alfvén waves are known to be capable of accelerating electrons by parallel electric fields especially close to the polar cap boundary (Paschmann et al., 2002), at arc boundaries, and during the expansive phase of substorms near midnight. The particle acceleration can be carried out by the formation of a parallel electric field at the wave front. In contrast to the inverted-V aurora, the parts of the aurora that are excited by Alfvén wave accelerated electrons are called "Alfvén wave aurora", or "Alfvénic Aurora" (Keiling, 2009). The roles, regions, and signatures of Alfvén waves in relation to the aurora will be reviewed in more detail in Chapter 4.

3.6 Acceleration region studies

The region in the space where the quasi-static auroral acceleration of charged particles takes place is called the *auroral acceleration region* (*AAR*). The spatial and temporal characteristics of the AAR are revealed more and more with the increasing knowledge on auroral processes and on the magnetosphere-ionosphere system. In the sections on the upward current region and on quasi-static electric fields, basic physics of the region was discussed. Here we briefly review the literature on the region along with some complementary notes on the in-situ observations by different spacecraft missions.

The existence of parallel electric fields in the auroral upward current region was first predicted theoretically by Alfvén (1958). Such fields were confirmed experimentally by McIlwain (1960) from the monoenergetic appearance of the electron spectra measured on a sounding rocket, which suggested acceleration by a parallel electric field. With the introduction of the space age, observing auroras at higher altitudes became possible. The first satellite confirmations were presented by Shelley et al. (1976) who found upward ion beams in the S3-3 data at an altitude of about 1 R_E, suggesting an acceleration region below this altitude. Mozer et al. (1977) made the first direct observations of very large quasi-static perpendicular electric fields on the S3-3 satellite at altitudes between 3000 and 8000 km. Since such large electric fields are not observed in the lower ionosphere, parallel electric fields are required to explain why they do not map down to low altitudes, i.e. the potential surfaces must close at some altitude above the ionosphere below the satellite, and thus be associated with parallel electric fields.

The acceleration process behind discrete aurora has been studied by single-satellite missions, such as S3-3 (Mozer et al., 1977), Viking (Lindqvist and Marklund, 1990;

Marklund, 1993), Dynamics Explorer 1 (DE1) (Weimer and Gurnett, 1993), FAST (Carlson et al., 1998) , and Polar (Mozer and Hull, 2001; Hull et al., 2003).

Direct identification of the parallel electric fields by single spacecraft has turned out to be extremely difficult, due to the relatively larger perpendicular electric field components combined with measurement limitations and uncertainties. Recalling that the total acceleration energy of auroral electrons may reach up to 10 keV, if the parallel potential is distributed over a broad altitude range, such as between 5000 and 8000 km, the average electric field would be on the order of 3 mV/m, which is small compared to the typical perpendicular components which are on the order of tens or hundreds of mV/m. Hence, in this case the direct measurement of the parallel electric field becomes very difficult. On the other limit, if the potential difference is concentrated to a very narrow altitude range, then the chances for (especially a single) satellite to arrive at the very altitude of the potential difference become very small, and it becomes unlikely to directly observe a parallel electric field. Using multiple spacecraft, the potential difference between the different altitudes on the same field line can be obtained and constraints can be put on the (altitude-averaged) parallel electric field (Paper 2).

The two-satellite studies by the DE1/DE2 spacecraft increased the knowledge about the degree of coupling between high and low altitude electric fields as a function of scale size (Weimer, 1985), which depends on the scale size of the electric field, as noted before.

The evolution of potential structures in time or space can not be detected by single-spacecraft missions. To reveal the spatio-temporal features of the AAR like the life time (growth and decay time), shape, and altitude profile of the potential structures, almost simultaneous observations by multiple spacecraft at different altitudes are required. At altitudes above the AAR, the Cluster quartet have been extensively used (Marklund et al., 2001; Vaivads et al., 2003, Marklund et al., 2004; Karlsson et al., 2004; Johansson et al., 2004; Figueiredo et al., 2005; Marklund et al., 2007).

Utilizing the pearls-on-a-string configuration of the Cluster spacecraft, Marklund et al. (2001) illustrated the growth and decay processes of a diverging potential structure in a region of downward field-aligned current using data of the four sequentially passing Cluster satellites at a geocentric distance of 4.3 R_E. The growth and decay took about 3 and 1.5 minutes respectively in that case. They also suggested that the lifetime of a positive potential structure is related to the time it takes to evacuate the ionospheric electrons within the flux tube of the downward current, which depends on the FAC magnitude.

In the AAR a variety of patterns of potential structures can occur, which can develop, vanish or move. In the simplest case of a U-shaped quasi-static structure, understanding the height distribution of the parallel potentials needs multiple spacecraft at different heights. If two spacecraft traverse the same field line at a given moment, the potential difference between them along the field line can be measured at that specific moment. However, even such an ideal passage can not provide information on the time evolution of the structures. A short time delay between the two spacecraft can be beneficial for

estimating both the quasi-static potential drop and growth/decay/stability times of the structure (Paper 2).

Cluster is the first satellite mission to make multi-point measurements in the AAR. The orbit perigee altitude of the Cluster spacecraft was decreased gradually during a few months from more than 4 R_E in winter 2008 to less than 1.5 R_E in summer 2009, with coverage of different altitudes. This allowed for the first time the study of the AAR with multiple spacecraft inside the region. Benefiting from this opportunity, in Paper 1 we revealed for the first time, the 2-D acceleration potential pattern and stability of a quasi-static potential structure, comprising two main U-shaped and one S-shaped structure, which stayed stable for 5 minutes. In another event study in Paper 2, we estimated the growth and decay times of two U-shaped potential structures and also estimated the parallel potential drop and electric field for one of them which was rather stable.

Chapter 4

Alfvénic auroral activity, signatures and regions

In the previous chapter we briefly noted the Alfvén waves as one of the components in auroral electron acceleration. In this chapter we will have a more detailed look at these phenomena. After an introduction to the Alfvén waves, a brief summary reviewing the roles, regions, and characteristic signatures of these waves is presented, with a focus on the auroral zone and the AAR.

4.1 Alfvén waves

Shear Alfvén waves are oscillations of ions and the magnetic field, $\delta\mathbf{B}$, traveling with a speed of the local Alfvén velocity (Keiling, 2009). Since Alfvén waves are electromagnetic waves, they have an oscillating electric field, $\delta\mathbf{E}$, too. Both $\delta\mathbf{E}$ and $\delta\mathbf{B}$ oscillate perpendicular to the ambient magnetic field (hence, the word "shear"). Shear Alfvén waves are low-frequency waves ($\omega <$ ion gyrofrequency) and propagate along the background magnetic field. The dispersion relation for these waves in a homogeneous magnetic field, at large wavelengths, is $\omega = k_{//} V_A$; i.e. the waves are not dispersive. No parallel electric field is supported in the ideal MHD regime for these waves at large perpendicular scale sizes. In the magnetosphere however, shear Alfvén waves can become dispersive and provide a parallel electric (and magnetic) field when the perpendicular wavelength of the wave becomes small and comparable to either the electron inertial length ($\lambda_\perp \sim \lambda_e = c/\omega_{pe}$) or to the ion gyroradius ($\lambda_\perp \sim r_g = \sqrt{T/m_i}/\omega_{gi}$, where T is either the electron temperature or ion temperature.) (Stasiewicz et al., 2000). In the first case, which takes place in the lower (colder, strongly magnetized part of the) magnetosphere where $V_A >> V_{th}$, the inertial effects dominate and the wave is called the inertial shear Alfvén wave. In the second case, which takes place in the upper (hotter, less magnetized part of the) magnetosphere where $V_A << V_{th}$, the thermal effects dominate and the wave is called kinetic shear Alfvén wave. The name 'kinetic' indicates the non-zero perpendicular component of the wave vector, which makes a kinetic treatment of the wave necessary. The non-zero perpendicular wave number also implies propagation oblique to the magnetic field, hence the other commonly used term 'oblique Alfvén

waves' (Karlsson, 2012). These are the most common dispersive Alfvén waves in the magnetosphere (Fedorov et al., 2004; Borovsky, 1993; Goertz and Boswell, 1979; Stasiewicz et al. 2000).

Freja and FAST studies highlighted the importance of the Alfvén waves in the low-altitude magnetosphere, especially providing new insights on the Alfvénic electron acceleration (Louarn et al. 1994; Chaston et al., 1999; 2000; 2002; 2003; Andersson, 2002; Wygant et al., 2002). The significance of Alfvén waves was even more appreciated by covering the higher altitudes. Especially, the extent of the Alfvénic Poynting flux carried from the magnetotail into the AAR could be estimated (Wygant et al. 2000; Keiling et al., 2000, Keiling, 2009). The Polar spacecraft, with its 3-dimensional electric field measurements and an orbit of 4 to 7 R_E, utilized together with low-altitude measurements, allowed for such an estimation. Conjunction studies (and statistical studies using satellites at different altitudes) enhanced our knowledge of Alfvén wave dissipation along auroral field lines. FAST-Polar conjunction studies highlighted the role of Alfvén waves in the creation of the aurora. It is now evidenced that Alfvénic electron acceleration not only occurs in the AAR, but also above it, and possibly along the whole PSBL flux tube. Studies using the UVI imager on Polar have strengthened the case for the Alfvén wave coupling of the magnetosphere-ionosphere system over the entire auroral oval. The studies utilizing IMAGE (Imager for Magnetopause-to-Aurora Global Exploration) space imager together with FAST have provided further information regarding where in the auroral oval Alfvén waves contribute to the aurora (Keiling, 2009 and references therein). The Cluster mission especially with its multipoint measurement has recently been used to study the evolutions of the Alfvénic regions (Hull et al., 2010) and their interaction with quasi-static potential structures (Paper 3 and Paper 4).

4.2. Roles of Alfvén waves

Alfvén waves play many roles in the dynamics of the magnetosphere. These roles can be summarized into magnetosphere-ionosphere coupling, Energy transport (especially from the magnetotail towards the AAR during the energy release of stored magnetic field energy at times of substorm expansion), parallel electric field support, particle acceleration, energy dissipation, field-aligned currents, auroral arc creation, field-line resonance (FLR), ULF pulsations, substorm dynamics, energy cascade leading to wave turbulence or anomalous resistivity, and reconnection. The application of Alfvén waves extends far beyond the magnetosphere. For more details on each of these roles, which can also overlap, see Keiling (2009).

Regarding their role in the field-aligned currents, it is worth mentioning that Alfvén waves carry field-aligned currents and are also necessary for the establishment of quasi-static, field-aligned currents (Keiling, 2009). However, the process is not well understood yet.

The term FLR is used in two ways. First, the coupling process of fast mode waves and shear Alfvén waves at Alfvén velocity gradients perpendicular to the magnetic field direction. Second, it refers to standing Alfvén waves oscillating between two reflecting

boundaries at the eigen frequency of a particular magnetic field line (Keiling, 2009). Clear evidence from space now indicates that FLR exists. FLR is associated in various ways with substorms; for example, it can control luminosity fluctuations of the aurora, it can start at substorm onset and it might play a role in the triggering of substorms.

Recently, Kinetic Alfvén waves have been observed in the reconnection region, which demonstrates that Alfvén waves at small scales are also an energy sink for the reconnection process (Keiling, 2009). The full extent of their importance has not yet been observationally demonstrated, however.

4.3. Wave signatures of auroral Alfvénic activity

It can be shown that the relation between the Alfvén velocity, the perpendicular electric field δE, and the disturbance in the magnetic field δB, for a purely traveling non-dispersive Alfvén wave is:

$$\delta E/\delta B = \pm V_A = \pm 1/\mu_0 \Sigma_A \quad (4.1)$$

where Σ_A is called Alfvén conductance and the +(-) sign is applicable to propagation parallel (anti-parallel) to the background magnetic field.

The kinetic and inertial effects always increase the ratios above the Alfvén speed (Louarn et al. 1994; Wygant et al. 2002; Keiling, 2009). Inertial Alfvén waves with short perpendicular wavelengths have ratios much higher than the local Alfvén speed (Stasiewicz, 2000).

Since the first observation of the perpendicular (to the background magnetic field) electric fields observed by Mozer et al (1977), in contrast to the quasi-static potential structure model, small-scale kinetic Alfvén waves had been suggested to explain them (Goertz, 1984). Comparing the two sides of the equation (4.1) from independent measurements, is a method to identify Alfvén waves (Mallinckrodt and Carlson, 1978; Keiling, 2009) and to decide whether the event is quasi-static ($\delta E/\delta B \sim \pm 1/\mu_0 \Sigma_P$) or Alfvénic ($\delta E/\delta B \sim \pm V_A$). Since the Pedersen conductance is about two orders of magnitude larger than the Alfvén conductance defined above, the $\delta E/\delta B$ ratio should be much smaller in the quasi-static case (Paschmann et al., 2002) and qualitatively, lower ratios indicate some degree of connection to the ionosphere (Keiling, 2009). For typical ionospheric conditions ($\Sigma_P \sim$5-40 S) the ratio is 18 to140 km/s (Stasiewicz, 2000 and the references therein), while the Alfvén velocity is much higher in the auroral zone, being around 10^4 km/s at 4 R_E and 10^5 km/s at 2 R_E geocentric distance (Janhunen et al., 2006; Keiling, 2009). For standing waves the ratio is not equal to the Alfvén speed due to a 90º phase shift between the monochromatic $\delta \boldsymbol{E_x}$ and $\delta \boldsymbol{B_y}$ fields; which can be detected using the Hilbert transform (Keiling et al., 2001; Keiling, 2009). However, even with applying such techniques, the $\delta E/\delta B$ method can in practice turn out to be an oversimplification, as wave reflections can happen with constructive or destructive results on the fields, destroying the simple relation. The interaction of Alfvén waves of various temporal and spatial scales with the ionosphere or regions of parallel electric fields can lead to phase

relationships between $\delta\boldsymbol{E}$ and $\delta\boldsymbol{B}$ more complicated than just a 90º phase shift (Keiling, 2009). The $\delta E/\delta B$ ratios can be affected in unpredictable ways (Keiling, 2009; Lysak and Dum, 1983; Knudsen et al., 1992; Vogt and Haerendel, 1998; and Streltsov and Lotko, 2003). In addition, temporal evolution of Alfvén waves, driven by both the generator region and any region of interaction (e.g., the ionosphere and parallel electric field regions) makes their identification more complicated. Utilizing modeling techniques together with observations is also an indirect method for identifying Alfvén waves (Keiling, 2009). Considering the standing wave structure of the FLR, in any particular observation, the satellite could be at a node or antinode of the electric field structure, giving a ratio of zero or infinity (Keiling, 2009). Lysak (1998) discussed modeling results for different scenarios suggesting that the ratio is not always equal to the Alfvén speed and that for small-scale quasi-static structures (<10 km at the ionosphere) the ratio can be higher than the speed of light for a wide range of altitudes. Under certain conditions, the two processes can take on the same $\delta E/\delta B$ ratio depending on other parameters, which makes using the method impossible for those conditions. These conditions may well happen inside and close to the AAR at the oval boundaries, where both processes are expected to exist. Especially, temporal electron acceleration processes expected to dissipate the Alfvén wave energy at 3-4 R_E altitude (Janhunen, 2006; see below) may affect the ratio.

Another important quantity associated with Alfvén waves is the Poynting flux $\mathbf{S}=(\delta\mathbf{E}\times\delta\mathbf{B})/\mu_0$. It is the Poynting flux that carries the wave energy and that can be converted into particle energy during dissipation processes (Keiling, 2009). It also indicates the direction of the energy flow, which is not readily apparent in **E** and **B** measurements alone. The parameter has been shown to be correlated with auroral luminosity (e.g. Keiling, 2002). While the electrons gain energy from high altitudes to the lower, the Poynting flux decreases, most probably dissipating into the electron acceleration. Janhunen (2006) suggested that the altitude range for such a dissipation is concentrated between 3 to 4 R_E. The existence of the Poynting flux at a particular location does not reveal whether the flux will ever dissipate, or whether it will simply circulate indefinitely (Keiling, 2009). In the magnetosphere, the two sources for the $\delta\mathbf{E}$ and $\delta\mathbf{B}$, i.e. the Alfvén waves and quasi-static field-aligned currents that close in the ionosphere, both have magnetic and electric field perturbations with the same polarization and are associated with Poynting flux propagation along magnetic field lines. Both quasi-static potential structures and Alfvén waves can be present simultaneously, and can be superposed in the measured signal, and hence it can be challenging to separate the two contributions (Keiling, 2009).

4.4. Particle signatures of auroral Alfvénic activity

It is now well established that Alfvén waves accelerate electrons in the auroral zone (Hasegawa 1976; Chaston et al., 1999; 2000; 2002; 2003; Keiling, 2009). Knudsen (1996) suggested that in the Earth's auroral zone, the criteria for electron acceleration to be significant are met for spatial scales comparable to or less than 1 km. Kinetic and inertial Alfvén wave pulses carry a parallel electric field at their leading edge which can accelerate electrons to speeds of the order of V_A ; speeds up to 2 V_A can be reached via

other processes (Knudsen, 1996; Goertz and Boswell, 1979; Kletzing, 1994; Hui and Seyler, 1992).

In spite of the occasional disagreement among scientists about the identification of Alfvén waves versus quasi-static structures, their particle signatures are clearly distinguished. In the upward current regions, electrons are seen narrow in energy and broad in pitch angle distribution (i.e. the inverted-V signature). In the downward current regions, electrons are seen broad in energy and narrow in pitch angle (Paschmann et al., 2002). In (purely) Alfvénic regions, electrons are observed counter streaming, having a broad energy range and a lower value of peak energy. As an indirect method of identifying Alfvén waves, the presence of the broad-energy electrons and simultaneous turbulent wave fields has been used extensively (Gary et al., 1998, Chaston et al., 2002, 2003; Keiling, 2009).

4.5. Alfvénic regions

The plasma sheet (including PSBL and the CPS) is generally assumed to map into the auroral oval, with the lobe poleward of it and the plasmasphere equatorward of it. The two latter regions are not typically associated with aurora. Much of the aurora that is caused by Alfvén-wave-accelerated electrons is related to the poleward region of the auroral oval which maps to the PSBL. During substorms, energetic Alfvén waves are mostly confined to the PSBL region. No confirmed origin has been found for these waves yet. The reconnection site is one suggested origin (Keiling, 2009). Alfvén waves in the CPS very often appear in the form of FLR. Similar to PSBL, generation mechanisms for the Alfvén waves in the CPS are not completely understood and confirmed; remaining an active area of research (Keiling, 2009). The fact that the plasma sheet connects the auroral zone to the reconnection region and that the lobe-PSBL interface is the division between open and closed field lines in the magnetotail, make the PSBL a specially significant region in all magnetospheric regions, and the site of diverse phenomena. In addition, in auroral substorm physics, the PSBL is of great importance, for example, for being the site for different forms of energy transport contributing to the creation of the aurora (Keiling, 2009). The energy transport was predominantly thought to rely on kinetic energy carried by ion beams, and electromagnetic energy carried by quasi-static FACs. Recently, this view has been revised by new studies reporting large-amplitude Alfvén waves in the PSBL that carry significant Poynting flux towards the AAR. Additionally, evidence for energetic field-aligned electron acceleration inside the PSBL also adds to the number of energy carriers possibly contributing to the aurora (Keiling, 2009). Using full 3-dimensional measurements of **E** and **B** from the Polar spacecraft above the AAR at 4–7 R_E, Wygant et al. (2000) and Keiling et al. (2000) unambiguously identified Alfvén waves in the PSBL, with the $\delta E/\delta B$ ratio of ~10,000 km/s, which was comparable to the local Alfvén speed. In addition, they demonstrated that Alfvén waves carried significant Poynting flux towards Earth. Using Geotail at farther distances (>15 R_E), Angelopoulos et al. (2002) reported Alfvén waves with peak Poynting fluxes larger than the Polar results. These observations provided a link between the magnetotail and the auroral zone, and demonstrated that the PSBL plays an important role as a region containing significant Alfvénic energy flux (Keiling, 2009, and references therein). It is

now believed that most likely, the energy source for the small-scale auroral zone Alfvén waves is the PSBL Alfvén waves.

The auroral zone typically shows three characteristic acceleration regions which are dominated by upward FACs, downward FACs, or Alfvén waves (of which, the two former were discussed in the previous chapter). Figure 4.1 shows a typical poleward crossing satellite observation in these regions. The PCB magnetically maps to the PSBL (Lotko, 2007; Keiling, 2009), where strong Alfvénic activity has been recorded, with evidence of the resulted aurora.

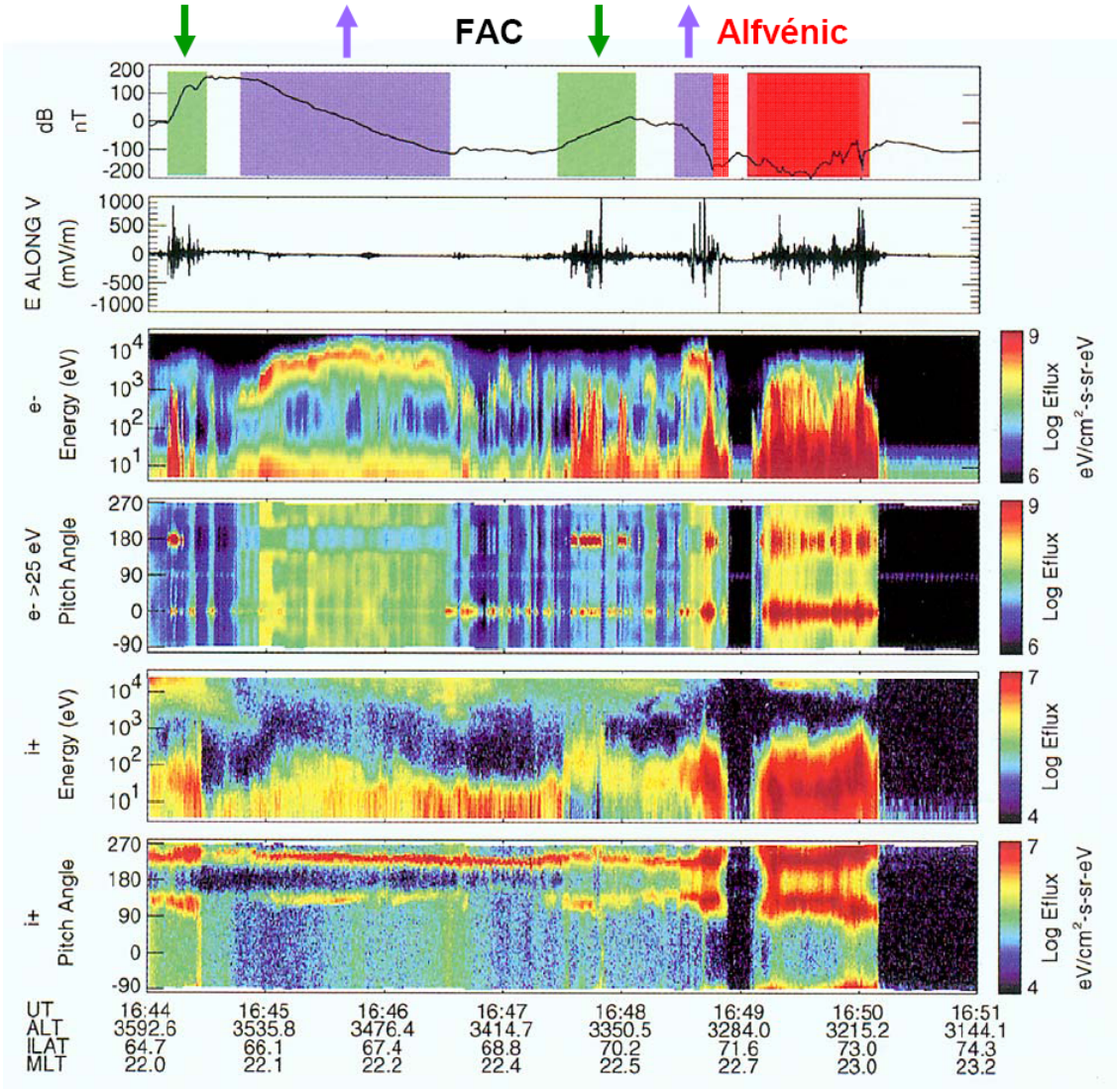

Figure 4.1: (From Lotko (2007), adapted from Paschman, 2002). An almost poleward pass by FAST spacecraft on February 13, 1997, across the premidnight Northern auroral zone at about 0.5 R_E altitude. The three characteristic acceleration regions are marked on the top panel: upward FAC with inverted-V (violet), downward FAC (green), and Alfvénic regions in the PCB (red).

Note the counter-streaming electron signature with broad energy range, characteristic of the Alfvénic activity dominating the PCB (marked by red color in the top panel).

Alfvénic fluctuations occur throughout the auroral zone, although they are most commonly found near the PCB (Keiling, 2009).

4.6. Alfvénic contribution to the aurora

Although there is now convincing observational evidence for the existence of both electrostatic and Alfvénic electric field structures, there is still a debate on their relative importance in various situations (Keiling, 2009). Statistical results roughly agree for the share of Alfvén waves in powering the aurora, being possibly up to one third on average and perhaps up to 50% in the pre-midnight region of the auroral oval. The Alfvénic contribution is dependent on geomagnetic activity with less contribution during quiet times (Keiling, 2009 and references therein).

4.7. Alfvénic- quasi-static interaction

It is not clearly understood if, where, to what extent, and how the quasi-static and Alfvénic acceleration processes coexist, or interact in the auroral zone. The former is dominant in the plasma sheet and especially in the CPS, while the latter is generally strongest in the PSBL. Using Cluster spacecraft at 4.4 geocentric radii and EISCAT radar, Aikio et al., (2004) presented evidence of Alfvénic downward acceleration of electrons in an upward current above an arc in the post-midnight sector. The energy of the electrons was too low (~200 eV) to create aurora; suggesting that additional acceleration (either quasi-static or Alfvénic) must have existed below the Cluster altitude. Under some circumstances, dispersive Alfvén waves can produce quasi-stationary structures (Aikio et al., 2004; Knudsen, 1996; Hui and Seyler, 1992; Streltsov and Lotko, 1999). Vaivads et al. (2003) observed signatures of both a quasi-static potential and an Alfvén wave in a conjugate study between Cluster located above the AAR (at 4.7 R_E) and DMSP located below the AAR (at 850 km). The authors suggested that the quasi-static potential structure might have been part of (the low-altitude end of) the Alfvén wave. As an example of evidence for co-existence of the quasi-static and Alfvénic signatures below the AAR, a study by Chaston et al. (2002) can be mentioned. They presented observations by FAST where the energy of an inverted-V peaking at 5–10 keV was modulated by the observed wave field, showing Alfvén waves in the inverted-V, and suggesting the propagation of an Alfvén wave from the outer magnetosphere into the AAR.

Temporal development is also a reason for confusion in separating electrostatic and Alfvénic structures. For example, any static field-aligned current structure must have started out as a dynamic, Alfvénic one and evolved into the static structure via an unknown sequence of processes (Keiling, 2009). The idea is that a sudden dynamic change in convection or resistivity in some region of the magnetosphere launches an Alfvén wave front. The front propagates back and forth between the source and any possible boundary, like the ionosphere. Before steady state is achieved, this interaction changes the Alfvén wave structure, sometimes disguising the Alfvénic origin. Eventually, a steady current will be set up, if one is created at all. Any new change in the ionospheric conditions or in the generator region will lead to additional Alfvén wave activity

(Keiling, 2009). It has also been suggested by theory/simulations and observations that the field-aligned currents carried by shear Alfvén waves may lead to the formation of some type of double layer on auroral field lines (Keiling, 2009). Such temporal variations can not be detected by single-spacecraft observations and will also affect the range and uncertainty in the statistical results based on these (e.g. on $\delta E/\delta B$ ratio). Hull et al. (2010) studied a Cluster spacecraft crossing at an altitude of ~3.5 R_E under very quiet geomagnetic conditions. Their results indicated that quasi-static systems of field-aligned currents may form out of the fine-scale Alfvénic regions at and just poleward of the PSBL.

In Paper 4, we observed regions of overlapping quasi-static and Alfvénic regions in which the Alfvénic electrons had energy-time distributions different from a purely Alfvénic signature. Although wave activity was observed and the broad-energy signatures existed in the electron spectrograms, the upgoing electrons had much lower energy fluxes and narrower energy ranges compared to the downgoing electrons. We propose that this results from the quasi-static potentials below and above the spacecraft affecting the Alfvénic signatures. The quasi-static upward electric field below the spacecraft reflects (the lower energy) part of the upgoing population back towards the ionosphere, so those reflected electrons will not reach the spacecraft, being one reason for the asymmetry. Also the quasi-static electric field above the spacecraft redirects part of the upgoing population back towards the (spacecraft and the) ionosphere, so in this way those reflected electrons are detected by the spacecraft, contributing to the downgoing electron population, hence strengthening the asymmetry.

Figure 6.2 gives a simplified visualization of a small-scale region of up- and down streaming electrons, showing how a purely Alfvénic (without a quasi-static component) signature typically looks like. Note that on a linear energy scale the energy distribution would be homogeneous for an ideal case (rather than looking denser at the higher energies). In this model, each electron is given an energy between $-U_A$ and U_A; where U_A is the peak acceleration energy that the Alfvén wave can provide in each direction, and the energy distribution is uniform.

Figure 6.3 represents the case with a quasi-static negative potential structure overlapping with the Alfvénic region. It should be emphasized that this is a rather simple model, just to show the first estimates of the situation, like the migration of upgoing electrons to the downgoing direction, and how the energy ranges might change for the two directions. In reality, what can be expected is perhaps the removal of the pitch angle ranges close to the upward direction in the energy-pitch angle spectrogram. However, the details of such a change highly depend on many parameters including the value of the quasi-static component, the value of the acceleration energy that the Alfvénic component delivers (both in the upward and downward directions), and the temperature of the electrons. In this model, each electron is given an additional quasi-static energy superposed on the Alfvénic value. The quasi-static component is normally distributed around an average value.

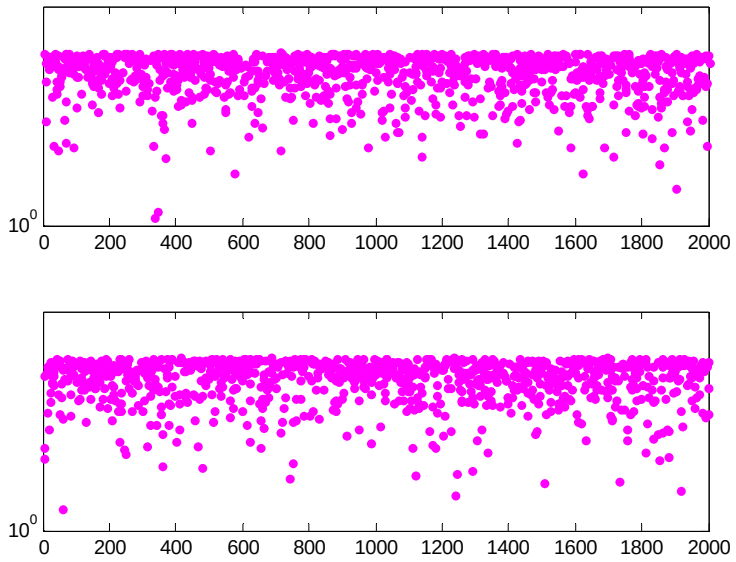

Figure 6.2) A visualization of Alfvénic signatures in energy-time electron spectrograms, when there is no co-existing quasi-static potential component. The energy scale (vertical axis) is logarithmic but the values are not written, as they can vary a lot. The horizontal axis can be regarded as spacecraft passage time. The top panel represents the upgoing electrons and the bottom panel the downgoing. The Alfvénic signature is symmetric.

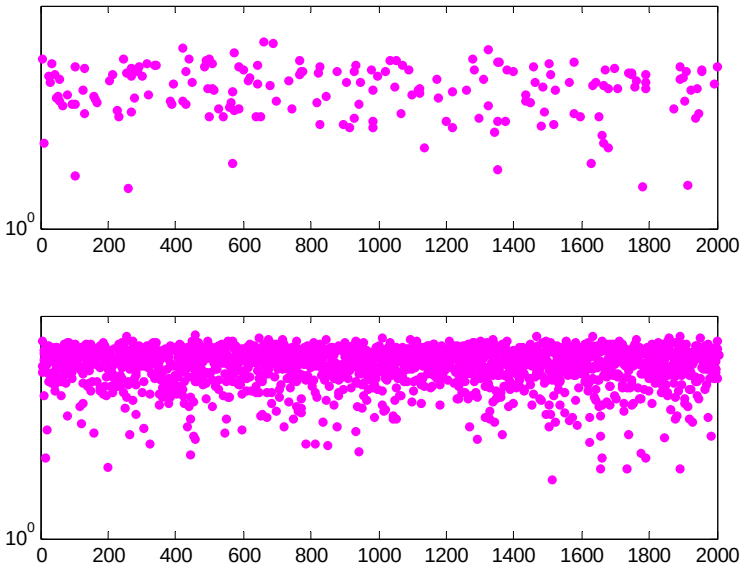

Figure 6.3) A visualization like figure 6.2, but for a case with a quasi-static component of upward parallel electric field co-existing with the Alfvénic acceleration. Note that as a result, the downgoing electrons are shifted to energies higher than for the previous case, the number of downgoing electrons is increased, and the number of upgoing electrons has decreased. The Alfvénic signature has become asymmetric by the quasi-static potential.

Chapter 5

The Cluster spacecraft

Cluster (II) is an ESA satellite mission in collaboration with NASA. The four identical satellites were launched in two pairs 16-Jul-2000 12:39 UT and 09-Aug-2000 11:13 UT on board two Suyoz-Fregat rockets from Baikonur, Kazakhstan. The mission had failed once in 1996, due to a software problem. The successful mission, which was planned to study the Earth's magnetosphere for two years, will be extended up to 2012, covering an entire solar cycle, and possibly up to 2014. The mission is one of the cornerstones of ESA's *Horizons 2000* programme. For the first time in space age, Cluster is collecting three-dimensional information on the solar wind-magnetosphere plasma environment. Figure 5.1 shows an overview of the Cluster orbits, especially comparing the orbits in 2001 and in 2009, the latter covering the AAR.

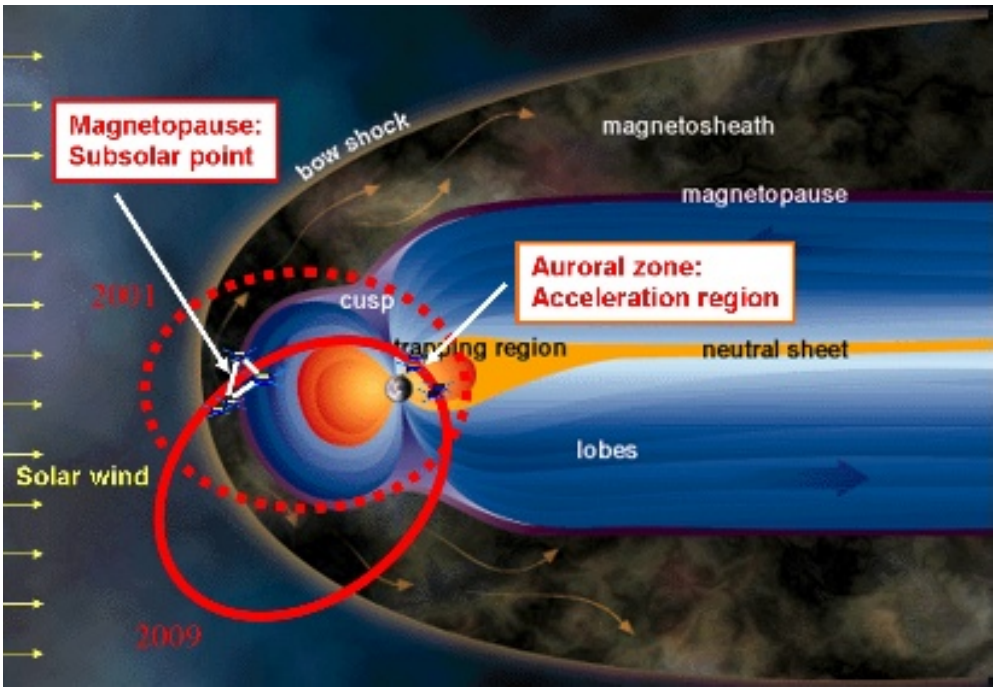

Figure 5.1: Cluster typical orbits in 2001 and 2009, and a diagram of the magnetosphere. Image credit: ESA.

The spacecraft are spin-stabilized with a spin period of 4 s. The spacecraft move in tetrahedral formation in a polar, highly elliptical orbit, with inter-spacecraft separations

varying between ~100 km to ~10000 km. The orbit period was ~57 hours and recently (in 2010) it was changed to ~54 hours. The formation in late 2008-early 2009 was a stretched tetrahedron with Cluster 3 lagging behind the others (e.g. by about 3 hours in February 2009). This lagging was gradually decreased, reaching about 20 minutes in early May and finally a few minutes in June. Each Cluster spacecraft has a disc-shaped cylinder form with a height of 1.3 m and diameter of 2.9 m. Each of the spacecraft is equipped with 11 instruments, as listed in Table 5.1. The main instruments used in this study are FGM, EFW, CIS, and PEACE; which will be briefly presented.

Abbreviation	**Instrument**
FGM	Fluxgate Magnetometer
EDI	Electron Drift Instrument
ASPOC	Active Spacecraft Potential Control experiment
STAFF	Spatio-Temporal Analysis of Field Fluctuation experiment
EFW	Electric Field and Wave experiment
DWP	Digital Wave Processing experiment
WHISPER	Waves of High Frequency and Sounder for Probing of Electron Density by Relaxation experiment
WBD	Wide Band Data instrument
PEACE	Plasma Electron And Current Experiment
CIS	Cluster Ion Spectrometry experiment
RAPID	Research with Adaptive Particle Imaging Detectors
WEC	Wave Experiment Consortium (WEC)

Table 5.1: Cluster instruments.

5.1 FGM

The magnetic field is measured by the Cluster FGM instrument (Balogh et al., 1997). Each instrument consists of two identical triaxial fluxgate magnetometers and an onboard data processing unit. Each sensor can be selected as the primary sensor. One of the two fluxgate magnetometers is located at the end of one of the 5.2 m radial booms (which is the default primary sensor) and the other one 1.5 meters inboard on the same boom, so as to be far away from the spacecraft magnetic field. The magnetic field is sampled at a rate of 15.519/18.341/22.416/67.249 vectors per second depending on the FGM instrument mode (Daly, 2008).

The magnetic field data from each single spacecraft can be used to calculate the FACs and their orientation assuming an infinite current sheet (Lindqvist, et al., 2010). One commonly used technique is called minimum variance analysis, abbreviated MVAB when applied to the magnetic field data. MVAB yields the direction in which the

variations in the magnetic field is minimum (i.e. finds the normal to the sheet), and the FAC density is then calculated from the gradient of the magnetic field component parallel to the sheet: $j_{//} = -\frac{1}{\mu_0}\frac{\partial B_t}{\partial x_n}$.
The infinite current sheet approximation is often applicable in the auroral region and we used it in Papers 1 to 4 to calculate the FACs and their deviation angles from the east-west direction. The MVAB technique is also a first step in other multi-spacecraft techniques of measuring the current and/or the current sheet properties: discontinuity analysis and the curlometer.

If the scale of the variations in the magnetic field is much smaller than the spacecraft separations, discontinuity analysis can be used to determine the curvature and/or motion of the structure (Dunlop et al., 2001; Daly, 2008). Karlsson et al. (2004) used Cluster FGM data and showed the feasibility of resolving the ambiguity of temporal versus spatial variations. Assuming a constant curvature and speed for the sheet, three spacecraft can suffice for calculating the speed vector and the curvature.

The curlometer technique (Dunlop et al., 2001; Daly, 2008) is applicable to estimate the current if the spacecraft are so close together that all are simultaneously located within the flux tube, (i.e. if the scale of the variations in the magnetic field is much larger than the spacecraft separations, so that the current inside the tetrahedron is constant). The technique calculates the three components of the current density by estimating the current through each face of the tetrahedron.

5.2 EFW

The Cluster EFW instrument (Gustafsson et al., 1997) consists of four spherical 8-cm-diameter probes which are extended on 42.5 m long wire booms with 88 m distance between each two opposite probes. Using the double-probe technique (Fahleson, 1967), the potential difference between the opposite probes is divided by the distance between them to obtain the two electric field components in the spin plane (Daly, 2008). The third component (i.e. the spin-axis component) of the electric field can be obtained from **E·B=0** (i.e. assuming $E_{//}=0$) if the magnetic field **B** is known and if the angle between the spin axis and **B** is large enough.

In the electric field measurement mode, the working point of the probe is optimized to yield the minimum impedance between the probe and the plasma, by feeding a fixed bias current to it. The probe potential will be determined by this current, the plasma electron current, and the photoemission current. This mode is also called current mode. In this case, to have an indicator of the ambient electron flux in a tenuous plasma, the potential difference between the probe (which is tried to be kept near the plasma potential) and the satellite body can be used. The resulting parameter, $U_{probe\text{-}sc}$ for each spacecraft is calculated from $U_{probe\text{-}sc} = U_{probe} - U_{sc}$; where U_{probe} is the average between the voltage values for all the probes working in this mode and U_{sc} is the spacecraft potential. The polarity of the $U_{probe\text{-}sc}$ parameter is hence such that a more negative value of $U_{probe\text{-}sc}$

corresponds to (a more positive spacecraft potential and) a lower plasma density (Daly, 2008).

In the density mode (voltage mode), theoretically a bias voltage can be applied to the probe with reference to the spacecraft ground. If the temperature is constant, applying a positive bias voltage to the probe will collect an electron current proportional to the plasma density, and hence the collected ambient thermal electron current can represent the variations in the plasma density. This method is rarely used, because of the high priority of the electric field measurements, and because of practical difficulties in measuring the resulting current.

Basically for each probe (numbered i), the voltage V_i (in the electric field mode) or current I_i (in density mode) can be sampled at rates between 5 to 36000 per second. Typically the voltages are sampled at 5 Hz. Potential differences V_{ij} are sampled at 25 Hz in normal mode and 450 Hz in burst mode. DC electric fields in the range 0.3-700 mV/m and AC electric fields in the frequency range 50-8000 Hz and amplitude range 0.001-10 mV/m can be measured.

The measured electric field also includes the electric field resulting from the motion and spinning of the spacecraft ($\mathbf{E_{V\times B}}$) and therefore needs removal of these effects. A 4 s resolution (spin-resolution) version of the EFW data is available from a least-square fit to the data over each spin period, which is the one we use in our papers.

Probe failures

The electric field is normally measured from V_{12} and V_{34}. The following probe failures have occurred (Lindqvist et al., 2010):
-probe1, spacecraft 1: on 28 December 2001
-probe1, spacecraft 3: on 29 July 2002
-probe1, spacecraft 2: on 13 May 2007
-probe 4, spacecraft 1: on 19 April 2009 (temporally, until 07 May 2009)
-probe 4, spacecraft 1: on 14 October 2009.
When a probe, e.g. probe 1, stops working, the V_{32} and V_{42} potential differences can be used instead of V_{12} to get the electric field. This asymmetric mode, of course, has larger errors due to the non-orthogonal signals used. The spin-resolution data need only one probe pair and are not affected.

5.3 CIS

The CIS instrument (Rème et al., 1997) obtains three dimensional ion distributions with spin-period time resolution and determines the mass-per-charge composition. It consists of two parts: COmposition and DIstribution Function (CODIF) and Hot Ion Analyzer (HIA).

1) http://www.mssl.ucl.ac.uk/missions/cluster/AAR_SP_home.php

The CODIF is a combination of an electrostatic analyzer and a subsequent time-of-flight analyzer. It is capable of mass-resolving of the major ion species, typically including H^+, He^+, He^{++}, O^{++}, within the energy range from the spacecraft potential up to 40 keV/e. In one spacecraft spin, it provides the full 4π ion distribution. The CODIF data have a minimum angular resolution of 22.5 º × 22.5 º.

The HIA works based on measuring the deflection of the ions in an electrostatic analyzer. It has an adequate angular resolution (5.6º × 5.6º) for ion beam and solar wind measurements (Daly, 2008). The CIS experiment on Cluster 2 is not operational.

Table 5.2 shows the CIS instrument status for the Cluster spacecraft as of May 2010 (Dandouras et al. 2010).

	SC 1	SC 2	SC 3	SC 4
CODIF	Operations until Oct. 2004	Not Operational	One deficient MCP quadrant until switch-off in Nov. 2009	Normal operations
HIA	Normal operations		Normal operations until Nov. 2009	Switched OFF: reduced energy coverage

Table 5.2 The CIS instrument status for the Cluster spacecraft.

5.4 PEACE

The PEACE instrument (Johnstone et al., 1997), measures the 3D electron velocity distribution function. Each PEACE instrument consists of two sensors, which basically can be used interchangeably, but one (the LEEA, Low Energy Electron Analyzer) is more appropriate for studies of high fluxes of low-energy electrons, and the other one (the HEEA, High Energy Electron Analyzer) is more suitable for high-energy electron fluxes. Each sensor is mounted on one side of the spacecraft and covers the full 4π solid angle in each spin. In the standard operation mode, the energy range (typically from 10 eV/e or from the anticipated spacecraft potential) up to 1.2 keV is covered by LEEA and with an overlap, the range 34 eV- 26.5 keV is covered by HEEA. Both LEEA and HEEA have an angular resolution of 15º in the polar direction. The angular resolution in the azimuthal direction is 2.8º for LEEA and 5.3º for HEEA.

Chapter 6

Summary of papers

6.1 Paper 1

Altitude Distribution of the Auroral Acceleration Potential Determined from Cluster Satellite Data at Different Heights

The event in paper 1 uses data from a dusk-toward-noon passage of Cluster over the auroral oval. We determine the 2-D morphology and altitude distribution of the acceleration potential above the aurora and address its stability in space and time. In this event, clear signatures of acceleration in electric field, magnetic field, ion data and electron data were observed by Cluster 1 (at altitude ~1.4 R_E) and Cluster 3 (at ~1 R_E). Cluster 3 was leading Cluster 1 by about 5 minutes, and the potential structure pattern was synthesized from the data from these two spacecraft. It comprises two U-shaped potential structures embedded in a larger one, and a narrower S-shaped potential structure below them (Figure 6.1). The ionospheric width of each of the two U-shaped structures remains steady (~100-120 km for the first one and ~140-150 km for the second one). In addition, their total acceleration potentials, inferred from the electric field data and from the particle data are almost steady (~4 kV for the first one and ~6-7 kV for the second one) and the structure is stable on a 5 minute time scale. The S-shaped structure is coinciding with the sharper density gradient. The pattern derived also shows that in the lower parts, the scale size of the electric field is much smaller than that of the FAC, as commonly reported on in the literature but not well understood, while the two scale sizes are roughly equal in the upper parts of the AAR.

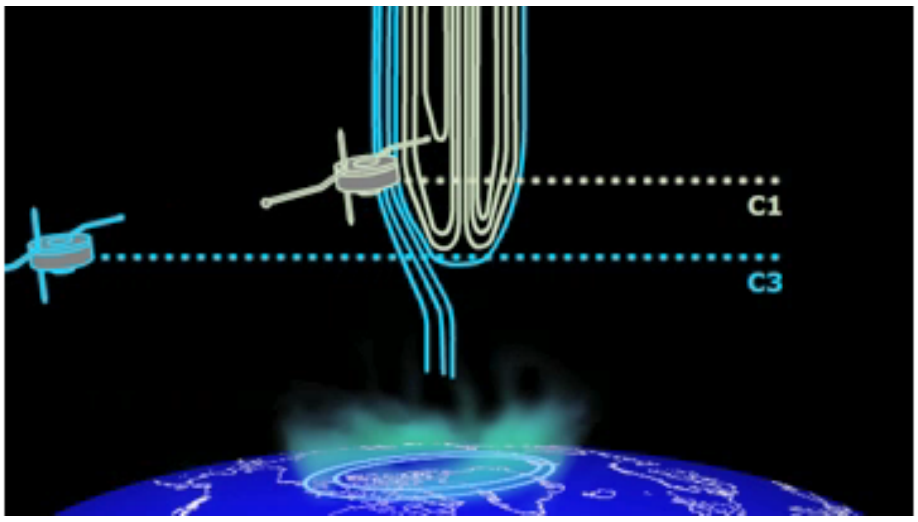

Figure 6.1 Cluster spacecraft 1 and 3 passing through the auroral acceleration region, resolving its altitude distribution and stability as in Paper 1 (Image adapted from ESA).

(For this event, Cluster 2 had no ion data and its trajectory was relatively far away from those of Cluster 1 and Cluster 3. Therefore we did not include data from it. Cluster 4 had no ion data of acceptable quality, either. It was leading Cluster 3 by about 1.5 minutes, and did not observe any clear signatures as Cluster 1 and 3. Hence, the only information we could obtain from Cluster 4 was that most probably the structure did not exist at the time of Cluster 4 crossing and was created in the 1.5 minutes between the Cluster 4 and Cluster 3 crossings.)

6.2 Paper 2

Spatio-temporal Features of the Auroral Acceleration Region as Observed by Cluster

In Paper 2, we investigate a pair of negative electric potential structures associated with inverted-V aurora, using electric and magnetic field, ion and electron data from Cluster spacecraft 1, 2, 4 crossings of the AAR at different altitudes above the Northern hemisphere midnight auroral oval. Cluster 3 was moving about 3 hours behind these three and we do not include data from this spacecraft. The two observed negative potential structures had total parallel potential drops of ~3 kV, converging electric fields of about 140 and 420 mV/m, and upward field-aligned currents of about 2 $\mu A/m^2$ (mapped down to the ionosphere) at the time of their maximum strength, and were associated with inverted-V electrons and up-going ion beams. The spatial and temporal evolution of the acceleration structures is studied, given the magnetic conjunction opportunity and the one minute difference between the Cluster spacecraft crossings. The configuration allowed for estimating the characteristic times of development for the two structures and estimating the parallel electric field and potential drop for the more stable one. The first potential structure had a normal width of ~80 km (mapped to the ionosphere) and was relatively short-lived, developing in less than 40 seconds and decaying in one minute. The parallel potential drop increased between altitudes of 1.13 R_E and 1.3 R_E, whereas the acceleration potential above 1.3 R_E remained almost unchanged during that time. This intensification occurred mainly after that the associated upward current had reached its maximum value. The second structure had a normal width of ~50 km and was subject to an increase by a factor of 3 of the parallel potential drop below 1.3 R_E, during about 40 seconds, after which it remained rather stable for one minute or more. Also here, the acceleration potential above 1.3 R_E remained roughly unchanged. For the more stable structure 2, a parallel potential drop of ~0.6 kV and an average parallel electric field of 0.56 mV/m between 1.13 R_E (Cluster 4) and 1.3 R_E (Cluster 1) were estimated. The spacecraft were conjugate within 0.3 degrees ILat, 0.16 hrs MLT.

6.3 Paper 3

Evolution in space and time of the quasi-static acceleration potential of inverted-V aurora and its interaction with Alfvénic boundary processes

In Paper 3, results are presented from Cluster crossings of the upper acceleration region of two inverted-V auroras located in the poleward part of a substorm bulge. The particle

and field data are used to infer the acceleration potentials of the arcs and their distribution in altitude and latitude. The Cluster 1 data demonstrate a symmetric potential pattern, composed of two negative U-shaped potential structures and one positive U-shaped potential in between, and the Cluster 3 and Cluster 4 data are consistent with an asymmetric pattern, where the dominating potential structure extends deep into the PCB region. Cluster 1 orbit projection is slightly to the east of those of Cluster 3 and Cluster 4. The two patterns may either correspond to different stages of evolution of the same double arc system or represent two longitudinally separated double arc systems. For all spacecraft, the potential well of the poleward arc extends into the PCB region, whereas the density cavity does not, but remains confined to Region 1. The results show that Alfvénic and quasi-static acceleration operate jointly in the PCB region, varying from being about equally important (on Cluster 1) to being predominantly quasi-static (on Cluster 3/Cluster 4). The deepest potential well of 13 kV observed by Cluster 4 was located in Region 1, adjacent to the PCB region and coinciding with the deepest density cavity. The presence of an upward electron beam, associated with a positive potential structure and a downward current, observed by Cluster 1, and its absence a few minutes later at the time of Cluster 4/Cluster 3 passages, is in agreement with the predicted life-time of these structures (Marklund et al., 2001).

6.4 Paper 4

Cluster Observations of Quasi-Static Potential Structures Overlapping With Alfvénic Regions

In paper 4 we present results from an equatorward crossing of the Cluster spacecraft through the high-altitude auroral acceleration region, over a system of East-West aligned auroral arcs in the Southern hemisphere auroral oval. The event occurred during quiet geomagnetic conditions during the expansion phase of a weak substorm. In addition to the data from all Cluster spacecraft, we use a UV image taken by the DMSP F17 satellite, passing just a few minutes after the latest arriving Cluster spacecraft, providing an overall picture of the oval regions crossed by each Cluster spacecraft. Acceleration potential profiles of the quasi-static structures are determined from the particle and field data. The observations reveal a dynamically developing system of small-scale and large-scale quasi-static structures overlapping with Alfvénic regions. Overlaps are found in three sites: In the poleward part of the PSBL, we observe Alfvénic signatures co-existing with small-scale negative and positive potential structures. In the equatorward part of the PSBL, i.e. at the PSBL/CPS interface, we observe Alfvénic signatures overlapping with the large-scale negative potential structure which corresponds to the Region 1 upward currents (combined with Region 0). In the Region 2 of downward currents, Alfvénic signatures co-exist with small-scale potential structures. No density cavities are seen in the overlap regions, similar to what was reported in Paper 3. Growths of small-scale potential structures were observed in the poleward part of PSBL and in the middle of Region 2, during the ~1.5 minutes between the Cluster 4 and Cluster 3 passages. During this period, the Alfvénic regions retreated both at the poleward and equatorward oval boundaries, and the large-scale quasi-static potentials intensified. The weakening/vanishing of Alfvénic signatures might be due to the dissipation of Alfvénic

wave energy into the enhancement of quasi-static potential, especially noting that it took place in the altitude range expected.

Chapter 7

Future work

The Cluster database now includes more than eleven years of prepared data and about one year of data currently being processed and prepared by different Cluster PI teams. The time period of the AAR crossings lies in between, with data prepared up to May 2010 and more to be added. Some ideas of future studies regarding Papers 1 to 4 are given below.

In paper 1, the parallel potential drops of the two U-potentials were confined at altitudes between Cluster 3 and Cluster 1, whereas that associated with the S-potential was located at lower altitude. More event studies of the potential distributions of the AAR are needed to verify whether this is a common feature or not. Since S-potentials are partly coupled to the ionosphere, which is not the case for U-potentials (which are totally decoupled) this suggests that the S-potential should be formed at a lower altitude when part of a combined potential structure. Another issue is the stability of the structures. Is the 5 min time scale typical for a large-scale potential structure, or it is simply one of a wide range of possible stability times? In Paper 1, it was also found that the ratio between the scale size of the electric field to that of the upward FAC channel was small in the lower part of the combined structure, and about one in the central parts of AAR. This result may be directly tied to the morphology of the U-and S-shaped potentials, but this needs to be examined further by studying more data from Cluster crossings of the AAR or results from other satellite missions reported on in the literature.

In Paper 2, the plasma density variations, indicated by the negative of the spacecraft potential, did not reveal the expected density cavities within the AAR of upward current regions. This matter can be investigated in more detail, for example by calibrating the relative density variations inferred from the spacecraft potential by WHISPER data. This could in addition be used to verify the Knight relation for the stable structure 2, providing more constrained information on the plasma density. The intensification of the parallel potential at the bottom of the structure 1 took place mainly after the build-up of the FAC. How often does this happen? How do the FAC and the parallel potential fit with the Knight relation for various phases of evolution of the structures? It would be of interest to further address the open issue of the altitude distribution of the parallel electric field and potential, whether they are distributed over a broad altitude range, or concentrated in narrow layers, the latter of which has been indicated by FAST observations and numerical simulation results.

The relative role of Alfvénic and quasi-static acceleration is a central but still far from resolved issue. Recent findings indicate that Alfvénic aurora may evolve into quasi-static aurora (Hull et al., 2010), or that the two types might operate in the same region jointly (Chaston et al, 2002; Aikio, 2004). This issue was addressed in Papers 3 and 4. Paper 3 focused on aurora close to the polar cap boundary, which is commonly believed to be predominantly Alfvénic. In both papers the Cluster data were supplemented by imager data. Paper 3 reported on the joint operation of the two processes at the PCB/Region 1 interface, and presented evidence of the efficiency of the joint acceleration processes. An important question here is how common such penetrations of potential structures into the PCB are, and whether the penetration into the PCB at times may be complete.

In paper 4, we saw overlaps between Alfvénic and quasi-static regions in three sites: in the poleward part of the PSBL, in the equatorward part of the PSBL and in the Region 2 of downward currents. A first question would be whether such overlaps are a common feature or not, which can be resolved by studying data from a large number of Cluster AAR crossings. A related question is whether the weakening of Alfvénic signatures and the growth of the quasi-static potentials are coupled to each other or not, with parallels to the abovementioned idea that Alfvénic structures may evolve into quasi-static potentials. What is the relative role of Alfvénic to quasi-static acceleration for various altitudes with respect to the AAR? What is the reason for the retreat of the Alfvénic regions and during what conditions is this seen? Do the temporal variations occur on the same few-minute time scale, as observed in Paper 4? Are there cases where density cavities co-exist with Alfvénic signatures? Similar event studies might shed more light upon these questions, especially if they can be combined by modeling results in each specific case. Studying a high number of similar events could be the next step in seeking answers for each of these questions.

Bibliography

A. Aikio, K. Mursula, S. Buchert, F. Forme, O. Amm, G. Marklund, M. Dunlop, D. Fontaine, A. Vaivads, and A. Fazakerley (2004). Temporal evolution of two auroral arcs as measured by the Cluster satellite and coordinated ground-based instruments, Ann. Geophys., 22, 4089–4101.

L. Andersson, J.-E. Wahlund, J. Clemmons, B. Gustavsson, and L. Eliasson (2002). Electromagnetic waves and bursty electron acceleration: implications from Freja, Ann. Geophys., 20: 139–150,

H. Alfvén (1942). Existence of Electromagnetic-Hydrodynamic Waves. Nature, 150, 405–406.

H. Alfvén (1958). On the theory of magnetic storms and aurora, Tellus, 10, 104.

H. Alfvén and C.-G. Fälthammar (1963). Cosmical Electrodynamics, Clarendon Press, Oxford.

V. Angelopoulos, J.A. Chapman, F.S. Mozer, J.D. Scudder, C.T. Russell, K. Tsuruda, T. Mukai, T.J. Hughes, K. Yumoto (2002). Plasma sheet electromagnetic power generation and its dissipation along auroral field lines. J. Geophys. Res. 107(A8), 1181, doi:10.1029/2001JA900136.

A. Balogh, M. W. Dunlop, S. W. H. Cowley, D. J. Southwood, J. G. Thomlinsson, K. H. Glassmeier, G. Musmann, H. Lühr, S. Buchert, M.H. Acuna, D.H. Fairfield, J.A. Slavin, W. Riedel, K. Schwingenschuh, and M.G. Kievelson (1997). The Cluster magnetic investigation. Space Sci. Rev., 79/1-2:65-91.

W. Baumjohann and R. A. Treumann (1999). Basic space plasma physics, Imperial College Press, London.

L. P. Block (1984). Three-dimensional potential structure associated with Birkeland currents. AGU Geophysical Monograph 28, Ed. T. Potemra (Proc. Chapman Conf. on Magnetospheric Current Systems, Irvington, Virginia, April 5-8, 1983), 28, 315-324.

J. E. Borovsky (1993). Auroral arc thickness as predicted by various theories. J. Geophys. Res., 98:6101-6138.

A. Brekke (1997). Physics of the upper polar atmosphere, Wiley.

C. W. Carlson et al. (1998). FAST observations in the downward auroral current region: energetic upgoing electron beams, parallel potential drops, and ion heating. Geophys. Res. Lett. 25, 12, 2017-2020.

C. C. Chaston, C. W. Carlson, W. J. Peria, R. E. Ergun and J.P. McFadden (1999). FAST observations of inertial Alfven waves in the dayside aurora, Geophys. Res. Lett. 26, NO.6, 647-650.

C.C. Chaston, C.W. Carlson, R.E. Ergun, J.P. McFadden (2000). Alfvén waves, density cavities and electron acceleration observed from the FAST spacecraft. Phys. Scr. T 84, 64.

C.C. Chaston, J.W. Bonnell, L.M. Peticolas, C.W. Carlson, R.E. Ergun, and J.P. McFadden (2002). Driven Alfvén waves and electron acceleration: A FAST case study. Geophys. Res. Lett.. doi:10.1029/2001GL013842

C.C. Chaston, J.W. Bonnell, C.W. Carlson, J.P. McFadden, R.E. Ergun, R.J. Strangeway (2003). Properties of small scale Alfvén waves and accelerated electrons from FAST. J. Geophys. Res. 108(A4), 8003, doi:10.1029/2002JA009420.

C. Chaston (2009). Auroral Particle Acceleration. Slide presentation at Nagoya University International GCOE School for "Particle acceleration in the Universe", http://www.gcoe.phys.nagoya-u.ac.jp/pau2009/slides/Chaston.pdf

F. F. Chen (1984). Introduction to Plasma Physics, Second Edition, Springer.

J.M. Cornwall and Y.T. Chiu (1982). Ion Distribution Effects on the Structures and Mapping of Auroral Electrostatic Potentials. J. Geophys. Res., 87, 1517-1527.

P. W. Daly (2008). Users Guide to the Cluster Science Data System. ftp://ftp.estec.esa.nl/pub/csds/task_for/users_guide/csds_guide.html.

I. Dandouras et al. (2010). User Guide to the CIS measurements in the Cluster Active Archive. http://caa.estec.esa.int/documents/UG/CAA_EST_UG_CIS_v12.pdf

T. N. Davis and T. J. Hallinan (1976). Auroral Spirals, I: Observations, J. Geophys. Res., 81, 3953-3958, 1976.

M. W. Dunlop, A. Balogh (2001). and K.-H. Glassmeier (2001). First Application of Multi-Point Magnetic Field Analysis Techniques: The curlometer and The Discontinuity Analyser. Sheffield Space Plasma Meeting: Multipoint Measurements versus Theory, Les Woolliscroft Memorial Conference held 24-26 April, 2001 in Sheffield, UK. Eurpoean Space Agency, 2001.

R. E. Ergun et al. (2000). Parallel electric fields in discrete arcs. Geophys. Res. Lett., 27, 4053-4056.

R. E. Ergun et al. (2001a). Direct Observation of Localized Parallel Electric Fields in a Space Plasma. Phys. Rev. Lett., 87, 045003-1-045003-4.

R. E. Ergun, Y.-J. Su, L. Andersson, C.W. Carlsson, J.P. McFadden, F.S. Mozer, D.L. Newman, M.V. Goldman, and R.J. Strangeway (2001b). Direct observations of localized parallel electric fields in a space plasma. Phys. Resv. Lett., Vol. 87, No. 4, 045003, 1-4.

U. Fahleson (1967). Theory of electric field measurements conducted in the magnetosphere with electric probes. Space Sci. Rev., 7:238-262.

E. N. Fedorov, V. A. Pilipenko, M. J. Engebretson, and T. J. Rosenberg (2004). Alfvén wave modulation of the auroral acceleration region. Earth Planets Space, 56, 649–661.

S. Figueiredo, G. Marklund, T. Karlsson, T. Johansson, Y. Ebihara, M. Ejiri, N. Ivchenko, P.-A. Lindqvist, H. Nilsson, and A. Fazakerley (2005). Temporal and spatial evolution of discrete auroral arcs as seen by Cluster. Ann. Geophys., 23:2531 - 2557.

C.-G. Fälthammar (2004). Magnetic-field aligned electric fields in collisionless space plasmas- A brief review. Geofisica Internacional, April-June, Vol. 43, Special issue- (Part B), 225-239.

J.B. Gary et al. (1998). Identification of auroral oval boundaries from in situ magnetic field measurements. J. Geophys. Res. 103, 4187.

C. K. Goertz and R. W. Boswell (1979). On the Proper Motion of Auroral Arcs. J. Geophys. Res., 98: 6087-6099.

C.K. Goertz (1984). Kinetic Alfvén waves on auroral field lines. Planet. Space Sci. 32, 1387–1392

D. A. Gurnett (1972).'INJUN 5 Observations of Magnetospheric electric fields and Plasma Convection'. In: B. M. McCormac (ed.): Earth's Magnetospheric Processes, Vol. 32 of ASSL. P. 233.

G. Gustafsson, R. Boström, B. Holback, G. Holmgren, A. Lundgren, K. Stasiewicz, L. Åhlén, F.S. Mozer, D. Pankow, P. Harvey, P. Berg, R. Ulrich, A. Pedersen, R. Schmidt, A. Butler, A.W.C. Fransen, D. Klinge, M. Thomsen, C.-G. Fälthammar, P.-A. Lindqvist, S. Christenson, J. Holtet, B. Lybekk, T.A. Stein, P. Tanskanen, K. Lappalainen, and J. Wygant (1997). The electric field and wave experiment for the Cluster mission. Space Sci. Rev., 79/1-2: 137-156.

T. Hallinan and T. Davis (1970). Small-scale auroral arc distortions. Planet. Space Sci. 18: 1735.

T. Hallinan (1976). 'Auroral Spirals, II: Theory'. J. Geophys. Res. 81, 3959.

A. Hasegawa (1976). Particle acceleration by MHD surface wave and formation of aurora. J. Geophys. Res. 811, 5083–5090.

T. W. Hill and A. J. Dessler (1991). Plasma motions in planetary magnetospheres. Science, 252:410.

C. H. Hui and C.E. Seyler (1992). Electron acceleration by Alfvén Waves in the magnetosphere. J. Geophys. Res., 97, 3953.

A. J Hull, J. W. Bonnell, and F., S. Mozer (2003). A statistical study of large-amplitude parallel electric fields in the upward current region of the auroral acceleration region, J. Geophys. Res., 108, SMP 5, 1-23.

A. J. Hull, M. Wilber, C. C. Chaston, J. W. Bonnell, J. P. McFadden, F. S. Mozer, M. Fillingim, and M. L. Goldstein (2010). Time development of field-aligned currents, potential drops, and plasma associated with an auroral poleward boundary intensification, J. Geophys. Res., 115, A06211, doi:10.1029/2009JA014651

B. Hultqvist (1971). On the production of a magnetic-field-aligned electric field by the interaction between the hot magnetospheric plasma and the cold ionosphere. Planet. Space Sci., 19, 749-759.

B. Hultqvist (1999). Acceleration of Ionospheric Outflowing Ions, Phys. Chem. Earth (C), 24, 247-257.

B. Hultqvist (2002). Downward ion acceleration at auroral latitudes: cause of parallel electric field, Ann. Geophys., 20, 1117–1136.

B. Hultqvist (2008). On the importance of auroral processes in the Universe. Journal of Atmospheric and Solar-Terrestrial Physics 70, 2235– 2245.

T. Iijima and T.A. Poterma (1978). Large-scale characteristics of field-aligned currents associated with substorms. J. Geophys. Res., 83:599-615.

P. Janhunen and A. Olsson (2000). New model for auroral acceleration: O-shaped potential structure cooperating with waves. Ann. Geophys., 18:596-607.

P. Janhunen, A. Olsson, C.T. Russell, and H. Laakso (2006). Alfvénic electron acceleration on aurora occurs in global Alfvén Resonosphere Region, Space Science Reviews 122: 89–95, DOI: 10.1007/s11214-006-7017-5.

T. Johansson et al. (2004). Intense high-altitude auroral electric fields – temporal and spatial characteristics, Ann. Geophys., 22, 2485–2495.

T. Johansson et al. (2006). On the profile of intense high-altitude auroral electric fields at magnetospheric boundaries. Ann. Geophys., 24, 1713-1723

A. D. Johnstone et al. (1997). PEACE: A plasma electron and current experiment. Space Sci. Rev., 19/1-2:351-398.

T. Karlsson and G. Marklund (1998). Simulations of effects of small-scale auroral current closure in the return current region. Physics of space plasmas, 15: 401-406.

T. Karlsson, et al. (2004). Separating spatial and temporal variations in auroral and magnetic fields by Cluster multipoint measurements, Ann. Geophys., 22, 2463–2472.

T. Karlsson (2012). The Acceleration Region of Stable Auroral Arcs, in Auroral Phenomenology and Magnetospheric Processes: Earth and Other Planets, Geophys. Monogr. Ser., vol. 197, edited by A. Keiling et al., AGU, Washington, D. C..

A. Keiling, J.R. Wygant, C. Cattell, M. Temerin, F.S. Mozer, C.A. Kletzing, J. Scudder, C.T. Russell, W. Lotko, A.V. Streltsov (2000). Large Alfvén wave power in the plasma sheet boundary layer during the expansion phase of substorms. Geophys. Res. Lett. 27, 3169.

A. Keiling, J.R. Wygant, C. Cattell, K.-H. Kim, C.T. Russell, D.K. Milling, M. Temerin, F.S. Mozer, C.A. Kletzing (2001). Pi2 pulsations observed with the Polar satellite and ground stations: Coupling of trapped and propagating fast mode waves to a midlatitude field line resonance. J. Geophys. Res. 106, 25,891.

A. Keiling, J.R. Wygant, C. Cattell, W. Peria, G. Parks, M. Temerin, F.S. Mozer, C.A. Kletzing (2002). Correlation of Alfvén wave poynting flux in the plasma sheet at 4–7 *RE* with ionospheric electron energy flux J. Geophys. Res. 107 (A7), 1132, doi:10.1029/2001JA900140

A. Keiling, J. R. Wygant, C. A. Cattell, F. S. Mozer, and C. T. Russell. (2003). The global morphology of wave Poynting flux: Powering the aurora. Science, 299: 383-386.

A. Keiling (2009). Alfvén Waves and Their Roles in the Dynamics of the Earth's Magnetotail: A Review. Space Sci. Rev. (2009) 142: 73–156.

C. A. Kletzing (1994). Electron acceleration by kinetic Alfvén waves. J. Geophys. Res. 99, 11, 095.

M. C. Kelley (1989). The Earth's Ionosphere, Vol. 43 of International Geophysics Series, San Diego, Academic Press.

J. Kimball and T.J. Hallinan (1998). Observations of black auroral patches and of thier relationship to other types of aurora. J. Geophys. Res., 103:14671-14682.

M.G. Kivelson and C.T. Russell (1995). Introduction to Space Physics.Cambridge, UK.

S. Knight (1973). Parallel electric fields, Planet. Space Sci., 21, 741.

D.J. Knudsen et al. (1992). Alfvén waves in the auroral ionosphere-A numerical model compared with measurements. J. Geophys. Res. 97, 77–90.

D.J. Knudsen (1996). Spatial modulation of electron energy and density by nonlinear stationary inertial Alfvén waves. 101, A5, 10761-10772.

J. Lemaire (1982). Advances in space research, Pergamon press PLC.

P.-A. Lindqvist and G. T. Marklund (1990). A Statistical Study of High-Altitude Electric Fields Measured on the Viking Satellite. J. Geophys. Res., VOL. 95, NO. A5, pp 5867-5876, May 1, 1990

P.-A. Lindqvist et al. (2010). User Guide to the EFW measurements in the Cluster Active Archive. http://caa.estec.esa.int/documents/UG/CAA_EST_UG_EFW_v30.pdf

W. Lotko (2007). The magnetosphere–ionosphere system from the perspective of plasma circulation: A tutorial, J. Atmos. Sol.-Terr. Phys. special issue on "Global Aspects of Magnetosphere-Ionosphere Coupling".

P. Louarn, J.-E. Wahlund, T. Chust, H. de Feraudy, A. Roux, B. Holback, P.O. Dovner, A.I. Eriksson, G. Holmgren (1994). Observations of kinetic Alfvén waves by the Freja satellite. Geophys. Res. Lett. 21, 195– 205.

L. R. Lyons (1992). Formation of auroral arcs via magnetosphere-ionosphere coupling. Rev. Geophys., 20, 2, May 1992, 93-112.

R.L. Lysak, C.T. Dum (1983). Dynamics of magnetosphereionosphere coupling including turbulent transport. J. Geophys. Res. 88, 365.

R. L. Lysak (1990). Electrodynamic coupling of the magnetosphere and ionosphere. Space Sci. Rev., 52, 33-87.

R.L. Lysak (1998). The relationship between electrostatic shocks and kinetic Alfvén waves. Geophys. Res. Lett. 25(12), 2089–2092.

A. J. Mallinckrodt and C. W. Carlson (1978). Relations Between Transverse Electric Fields and Field-Aligned Currents. J. Geophys. Res. 83, A4, 1426-1432.

G. Marklund (1984). Auroral arc classification scheme based on the observed arc associated electric field pattern. Planet. Space Sci., 32:193-211.

G. T. Marklund (1993). Viking Investigations of Auroral Electrodynamical Processes. J. Geophys. Res. 98, A2, 1961-1704.

G.T., Marklund, L.Blomberg, C.G. Fälthammar, and P.-A. Lindqvist (1994). On intense diverging electric fields associated with black aurora, Geophys. Res. Lett., 21, 17, 1859-1862.

G. Marklund, T. Karlsson, and J. Clemmons (1997). On low-altitude particle acceleration and intense electric fields and their relationship to black aurora, J. Geophys. Res., 102, A8, 17509–17 522.

G. Marklund, N. Ivchenko, T. Karlsson, A. Fazakerley, M. Dunlop, P.-A Lindquist., S. Buchert, C. Owen, M. Taylor, A. Vaivads, P. Carter, Andr´e, M., and A. Balogh (2001). Temporal evolution of the electric field accelerating electrons away from the auroral ionosphere, Nature, 414, 724–727.

G. Marklund et al. (2004). Characteristics of quasi-static potential structures observed in the auroral return current region by Cluster, Nonlinear Processes in Geophysics, 11, 709–720.

G. Marklund, , T. Johansson, S. Lileo, and T. Karlsson (2007). Cluster observations of an auroral potential and associated field-aligned current reconfiguration during thinning of the plasma sheet boundary layer, J. Geophys. Res, 112, A01208, 1-7.

C. E. McIlwain (1960). Direct measurement of particles producing visible auroras, J. Geophys. Res., 65, 2727–2747.

A. Morioka, Y. S. Miyoshi, F. Tsuchiya, H. Misawa, A. Kumamoto, H. Oya, H. Matsumoto, K. Hashimoto, and T. Mukai (2005). Auroral kilometric radiation activity during magnetically quiet periods, J. Geophys. Res., 110, A11223, doi: 10.1029/2005JA011204.

F. S. Mozer, C. W. Carlson, M. K. Hudson, R. B. Torbert, B. Parady, J. Yatteau, and M. C. Kelley (1977). Observations of paired electrostatic shocks in the polar magnetosphere, Phys. Rev. Lett., 38, 292-295.

F.S. Mozer and A. Hull (2001). Origin and geometry of upward parallel electric fields in the auroral acceleration region, J. Geophys. Res., 106, A4, 5763-5778.

NASA-Astronomy Picture Of the Day: http://apod.nasa.gov/apod/ap100701.html

A. Olsson (1997). Studies of Magnetosphere-Ionosphere coupling in auroral substorms using radar and satellite techniques. IRF scientific report, 240.

G. Paschmann, P. W. Daly (Eds.) (2001). Analysis Methods for Multi-Spacecraft Data. International Space Science Institute. Publisher: ESA Publications Division, Noordwijk, The Netherlands.

G. Paschmann, S. Haaland, and R. Treumann (Eds.) (2002). Auroral Plasma Physics. ISSI, Kluwer academic publishers.

H. Rème et al. (1997). The Cluster ion spectrometry (CIS) experiment. Space Sci. Rev., 19/1-2:303-350.

A, .D. Richmond et al. (1988). Mapping electrojet features of the high-latitude Ionosphere from localized observations: Combined incoherent scatter radar and magnetometer measurements for January18-19, 1984. J. Geophys. Res., 93, 5760.

E. G. Shelley, R. D. Sharp, and R. G. Johnson (1976). Satellite observations of an ionospheric acceleration mechanism, Geophys. Res. Lett., 3, 654–656.

K. Stasiewicz et al. (2000). Small scale Alfvénic structure in the aurora. Space Science Reviews, 92:423-533.

SouthWest university Research Institute (SWRI) Glossary: http://pluto.space.swri.edu/image/glossary/substorm.html

A.V. Streltsov, W. Lotko (1999). Small scale "electrostatic" auroral structures and Alfvén waves. J. Geophys. Res. 104, 4411–4426.

A.V. Streltsov and W. Lotko (2004). Multiscale electrodynamics of the ionosphere-magnetosphere system. J. Geophys. Res. doi:10.1029/2004JA010457.

A.V. Streltsov and G. Marklund, (2006). Divergent electric fields in downward current channels, J. Geophys. Res., 111, A07204, doi:10.1029/2005JA011196

A. Vaivads, M. Andre, S. Buchert, A.I. Eriksson, A. Olsson, J.-E. Wahlund, P. Janhunen, G. Marklund, L.M. Kistler, C. Mouikis, D. Winningham, A. Fazakerley, and P. Newell (2003). What high altitude observations tell us about the auroral acceleration: A Cluster/DMSP conjunction. Geophys. Res. Lett., 30, 3, 1106, doi:10.1029/2002GL016006.

J. Vogt and G. Haerendel (1998). Reflection and transmission of Alfvén waves at the auroral acceleration region. Geophys. Res. Lett. 25, 277.

D. R. Weimer and D. A. Gurnett (1993). Large-Amplitude Auroral Electric Fields Measured With DE 1. J. Geophys. Res., 98, A8, 13, 557-13, 564.

D. R. Weimer, C. K. Goertz, D. A. Gurnett, N. C. Maynard, and J. L. Burch (1985). Auroral Zone Electric Fields from DE 1 and 2 at Magnetic Conjunctions, J. Geophys. Res., 90, A8, 7479-7494.

Wikipedia: www.wikipedia.com

J. R.Wygant et al. (2000). Polar spacecraft based comparisons of intense electric fields and Poynting flux near and within the plasma sheet-tail lobe boundary to UVI images: An energy source for the aurora. J. Geophys. Res. 105, 18,675.

J.R.Wygant et al. (2002). Evidence for kinetic Alfvén waves and parallel electron energization at 4–6 *RE* altitudes in the plasma sheet boundary layer. J. Geophys. Res. 107(A8), 1201 doi:10.1029/2001JA900113.